

Contents lists available at ScienceDirect

Physica D

journal homepage: www.elsevier.com/locate/physd





Tipping in a low-dimensional model of a tropical cyclone

Katherine Slyman ^{a,*}, John A. Gemmer ^b, Nicholas K. Corak ^c, Claire Kiers ^d, Christopher K.R.T. Jones ^{d,e}

- ^a Division of Applied Mathematics, Brown University, Providence, RI 02906, United States of America
- b Department of Mathematics, Wake Forest University, Winston-Salem, NC 27109, United States of America
- ^c Department of Physics, Wake Forest University, Winston-Salem, NC 27109, United States of America
- d Department of Mathematics, University of North Carolina at Chapel Hill, Chapel Hill, NC 27599, United States of America
- ^e Department of Mathematics, George Mason University, Fairfax, VA 22030, United States of America

ARTICLE INFO

Keywords: Dynamical systems Rate-induced tipping Freidlin–Wentzell rate functional Noise-induced tipping Rare events

ABSTRACT

A presumed impact of global climate change is the increase in frequency and intensity of tropical cyclones. Due to the possible destruction that occurs when tropical cyclones make landfall, understanding their formation should be of mass interest. In 2017, Kerry Emanuel modeled tropical cyclone formation by developing a low-dimensional dynamical system which couples tangential wind speed of the eye-wall with the inner-core moisture. For physically relevant parameters, this dynamical system always contains three fixed points: a stable fixed point at the origin corresponding to a non-storm state, an additional asymptotically stable fixed point corresponding to a stable storm state, and a saddle corresponding to an unstable storm state. The goal of this work is to provide insight into the underlying mechanisms that govern the formation and suppression of tropical cyclones through both analytical arguments and numerical experiments. We present a case study of both rate and noise-induced tipping between the stable states, relating to the destabilization or formation of a tropical cyclone. While the stochastic system exhibits transitions both to and from the non-storm state, noise-induced tipping is more likely to form a storm, whereas rate-induced tipping is more likely to cause the storm to destabilize. In fact, rate-induced tipping can never lead to the formation of a storm when acting alone. When rate-induced tipping causes the storm to destabilize, a striking result is that both wind shear and maximal potential velocity have to increase at a substantial rate in order to affect tipping away from the active hurricane state. For storm formation through noise-induced tipping, we identify a specific direction along which the non-storm state is most likely to get activated.

1. Introduction

Tipping is the rapid, and often irreversible, change in the state of a system [1] and it is well understood that many elements of the climate system are particularly susceptible to tipping in some fashion [2,3]. There are other reasons to be concerned about tipping regarding climate change: it has played a role in the collapse of human societies, it exacerbates infectious disease spread and spillover risk, and it affects the severity of extreme weather events [4]. While much of the recent mathematical research on tipping has focused on climate applications, see for instance [5–11], it also has broad applications in ecology [12,13], ecosystems [14,15], epidemiology [16–19], and social systems [20,21]. Due to the diversity of important applications and the magnitude of the impacts of these phenomena, understanding the mathematics of tipping promises to have significant impact on many existing and recurring problems in our current society.

We present a study of the determination and classification of tipping events for a low-dimensional model of tropical cyclones. In this system, tipping events can be loosely defined as occurring when a sudden or small changes to a variable or parameter induces a large change to the state of the system in a short amount of time, e.g. the formation or destabilization of a storm. More precisely, in [22] it was proposed that tipping events could be predominately classified and studied from a mathematical perspective, according to whether they are induced by a classical bifurcation (B-tipping), a rate dependent parameter (R-tipping), or by noise (N-tipping); see Fig. 1 for a simplified schematic of these three classifications. These tipping mechanisms do not always act independently; a combination of different mechanisms can also lead to tipping. We specifically explore how parameter shifts and noise affect tipping within tropical cyclones. While in this work we provide

E-mail address: katherine_slyman@brown.edu (K. Slyman).

^{*} Corresponding author.

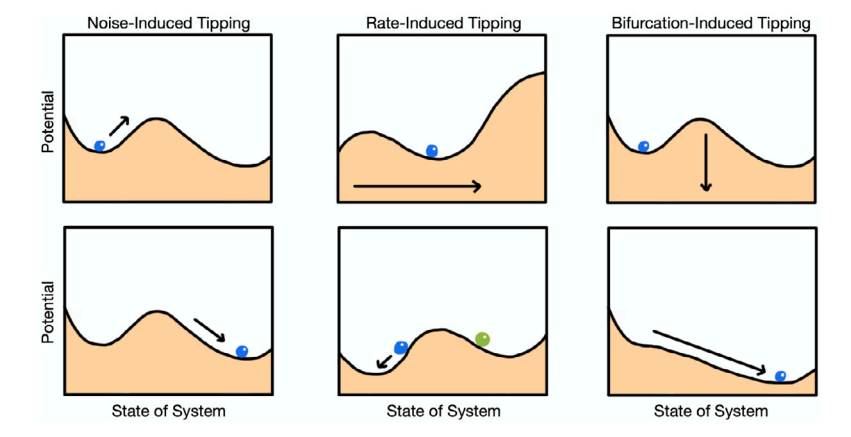


Fig. 1. Schematic diagram for noise, rate, and bifurcation-induced tipping in gradient systems when initializing with a particle at a minimum of the potential. For noise-induced tipping, the random fluctuations are needed for the system to overcome the energy barrier to move to another local minimum. In rate-induced tipping, the potential is moved horizontally at a quick enough rate so that the particle enters the basin of attraction of another local minimum. In bifurcation-induced tipping, the changing parameter eliminates the energy barrier allowing the particle to fall to the other local minimum. This figure is inspired and then recreated from [36].

a brief overview for these tipping mechanisms, we point the reader to [1,22–30] for a more thorough discussion.

Tropical cyclones, or hurricanes as they are referred to in the Northern Atlantic and Eastern Pacific basins, are complex storms characterized by their rapid rotation and heavy rains, and are some of the most costly of natural disasters both in terms of property damages and in lives lost [31]. Hurricane Dorian, one of the strongest tropical cyclones to make landfall in recent years, hit the Bahamas as a category 5 hurricane, sustaining winds over 185 miles per hour. It was responsible for an estimated \$7 billion in damages, over 400 dead or missing persons, and immeasurable losses to reef and mangroves, which in turn impacted tourism, the fishing industry, and protection from future storms [32]. In 2005, Hurricane Katrina struck the gulf coast of Louisiana and was one of the costliest storms on record, causing over \$125 billion, and over 1800 lives lost despite only sustaining winds of 127 mph upon landfall [33]. Across the globe, tropical cyclones can cause even more damage. It is estimated that the Philippines spend 5% of its GDP per year on damages from typhoons (tropical cyclones of the Pacific basin) [34]. A presumed impact of global climate change is the increase in frequency and intensity of tropical cyclones, e.g., if waters warm north of the equator, it could impact the frequency of tropical cyclone development and, in turn, locations of landfall. As an example, consider Hurricane Lorenzo of 2019 which made landfall in Ireland and was the easternmost Category 5 hurricane on record having impacts across the Atlantic [35]. Because of the destruction that can occur when tropical cyclones make landfall, understanding what mechanisms lead to their formation should be of interest to governments, risk analysts, and climate scientists.

1.1. Description of model

Tropical cyclones can be modeled as an axisymmetric vortex in hydrostatic equilibrium with a rotational velocity resulting from conservation of angular momentum [37,38]. Specifically, tropical cyclones form over warm water, generally between the Tropics of Capricorn and Cancer, in which there is a temperature gradient between the warm ocean and cooler lower atmosphere. Essentially, as warm water evaporates, the resulting warm air mass rises and cools rapidly releasing heat through condensation back into the atmosphere. As the warm air rises, an area of low pressure forms and air begins to move from all directions to fill this void. The air in this region swirls from the Coriolis effect and, due to conservation of angular momentum, eventually forms a rotating air mass around the area of low pressure, i.e., the eye of the storm.

Formulating a model capturing this effect, [39] derived an equation for the tangential wind speed $V \ge 0$ resulting from the competition

between the dissipation of kinetic energy and the power generated by the storm:

$$\frac{dV}{dt} = \frac{1}{2} \frac{C_d}{h} \left(V_{p0}^2 - V^2 \right),\tag{1}$$

where $C_d/h > 0$ has units of inverse length and couples the effect of surface drag and ocean boundary layer depth, i.e. the top depth of ocean that interacts with the bottom layer of the atmosphere [38]. The maximum potential velocity of the hurricane, $V_{p0} > 0$, is a parameter that is calculated by modeling the storm as a Carnot engine and equating the kinetic energy with the theoretical maximum power that could be sustained by the storm [38].

The model presented in Eq. (1) is limited in its applicability, as it does not account for environmental wind shear, dissipative heating, and surface-saturation specific humidity. A more realistic model accounting for these effects was developed in the work of Emanuel and Zhang [40], and Emanuel [41], and is given by

$$\frac{dV}{dt} = \frac{1}{2} \frac{C_d}{h} [(1 - \gamma)V_p^2 m^3 - (1 - \gamma m^3)V^2],$$

$$\frac{dm}{dt} = \frac{1}{2} \frac{C_d}{h} [(1 - m)V - 2.2Sm],$$
(2)

where $\gamma \in [0,1]$ is a dimensionless parameter accounting for dissipative heating and pressure dependence of the surface saturation humidity, $V_p^2=(1-\gamma)^{-1}V_{p0}^2$, and S is the wind shear measured in units of velocity. More specifically, $\gamma=(T_A-T_0)/T_0+\kappa$, where T_A,T_0 are the temperatures of the lower atmosphere and upper ocean respectively, κ is a constant and thus γ^{-1} is a proxy for the temperature of the ocean. Here, the dependent variable m can be thought of as relative humidity, thus dimensionless, and satisfies $m \in [0, 1]$. In this model, m serves as a "fuel" for the tropical storm, and indeed if m = 1, i.e. the core is fully saturated, we recover Eq. (1). The negative in front of the wind shear term reflects the role wind shear plays in pulling moisture out of the storm, leading to its possible dissipation. In this form of the model, the particular factor of 2.2 in front of the shear term and the cubic nonlinearities on moisture are empirical results from numerical experimentation [40]. Note, in [40,41] this model is presented with an ocean feedback term accounting for the fact that high velocity storms begin to pull up ocean water which cools the hurricane. This additional term does not significantly impact the qualitative behavior of this model, and thus to simplify the analysis we have chosen to neglect it. Note, for physically relevant parameters and nonzero wind shear, this dynamical system always contains a stable fixed point at the origin (V = 0, m = 0) corresponding to a non-storm state. For sufficiently low wind shear, it contains an additional asymptotically stable fixed point corresponding to a stable storm state as well as a saddle corresponding to an unstable storm state.

1.2. Summary of key results and organization of paper

In Section 2, we examine the dimensionless version of Eq. (2), lay out the parameter regimes of interest, perform a standard bifurcation analysis, and study the qualitative behavior of the model.

In Section 3, we present the basic theoretical framework for rate-induced tipping, study the possibility of rate-induced transitions between the non-storm and stable storm states, and conclude this section with a numerical example that illustrates rate-induced tipping. Creating a storm by tipping from the non-storm state to the stable storm state is never possible through rate-induced tipping alone due to the fact the non-storm state is stationary with respect to changes in parameters.

We prove that the deterministic system undergoes rate-induced tipping away from the stable storm state to the non-storm state. This will occur when the max potential velocity and the dimensionless wind shear both increase at a sufficiently high rate. A surprising and very interesting aspect of this result is that both maximal velocity and wind shear need to increase to cause tipping. It is not surprising that wind shear needs to increase as it is well-known that a lack of wind shear is necessary to support a hurricane. The maximum potential velocity of the storm is a proxy for the energy available to the storm. It is counterintuitive that it should have to increase to force a storm to end, rather than the other way around. While this may reveal a hidden flaw in such a low-dimensional model, it may also be a genuine effect in that increasing the maximum potential velocity implicitly requires the storm to be stronger to survive. If this requirement sets in too quickly then the storm may be unable to adjust. Therefore, in this model at least, a hurricane can destabilize due to rapidly changing parameters but can

In Section 4, we consider the addition of noise to the system and investigate transitions between the non-storm and stable storm states. We show the stochastic system exhibits tipping to and from the non-storm state, implying a hurricane can form or destabilize with the addition of random fluctuations acting on the system. The primary mathematical tool we use is the Freidlin-Wentzell theory of large deviations to determine the most probable transition path between states. In this framework, the most probable transition path can be computed as the minimum of an action functional which satisfies a Hamiltonian system of differential equations. By exploiting the Hamiltonian structure of these equations we are able to compute an asymptotic formula for the most probable transition path from the non-storm state to the stable storm state which further allowed us to estimate the expected tipping time from the non-storm state. To validate this approximation we compared our approximation with a direct gradient flow of the action functional. Monte Carlo simulations reveal the accuracy of the most probable path and also demonstrate the system's susceptibility to tipping.

However, while it is truly a rare event for noise to tip the system from the stable storm state to the non-storm state, we show that the stochastic system is highly susceptible to tip from the non-storm state to the stable storm state. Both analytical arguments and numerical experiments show that noise-induced tipping is needed (and likely) to form a storm whereas rate-induced tipping is a favored mechanism for destabilizing a storm.

Lastly, in Section 5, we discuss the implications and key significance of this work and discuss the interplay between the rate and noise-induced tipping mechanisms via numerical simulations. When considering the stochastic system, and also allowing both the max potential velocity and the dimensionless wind shear to be time-dependent parameters, the system again exhibits tipping to and from the nonstorm state. When the system tips from the non-storm state to the stable storm state, the two tipping mechanisms act independently: noise-induced tipping occurs before the ramp begins and then the system end-point tracks the stable storm state. However, when the system tips from the stable storm state to the non-storm state, there is an interplay of the two tipping mechanisms.

2. Analysis of autonomous system and bifurcation-induced tipping

To give context to the tipping results, we first perform a standard bifurcation analysis of Eq. (1) as well as study the qualitative behavior of the model. To do so, it is convenient to introduce the dimensionless variables $v=V/V_p$ and $\tau=C_d/(2h)V_pt$ which yield the dimensionless system given by

$$\frac{dv}{d\tau} = f(v, m) := (1 - \gamma)m^3 - (1 - \gamma m^3)v^2,
\frac{dm}{d\tau} = g(v, m) := (1 - m)v - cm,$$
(3)

where $c=2.2S/V_p$ is the dimensionless wind shear. Note, from the discussion of this model in the introduction, we expect that $0 \le V \le V_p$ and $0 \le m \le 1$ and thus the relevant phase space on which the forward flow of Eq. (3) should be defined is $\Pi = [0,1] \times [0,1]$. Indeed, since $\gamma \in (0,1)$, it follows that $f(0,m) \ge 0$, $f(1,m) \le 0$, $g(v,0) \ge 0$, $g(v,1) \le 0$ and thus Π is forward invariant.

The fixed points of Eq. (3) satisfy the system of equations m = v/(v+c) and $q(v) = v^2p(v) = 0$, where p is the cubic polynomial

$$p(v) = (1 - \gamma)v + \gamma v^3 - (v + c)^3.$$
(4)

Therefore, regardless of parameter values, the origin $\mathcal{O}=(0,0)$ (non-storm state) is a fixed point of Eq. (3). However, v=0 is a repeated root of the quintic polynomial q and thus \mathcal{O} is not a hyperbolic fixed point. Nevertheless, it can be shown through a center manifold reduction that the origin is in fact a stable fixed point; see Appendix B.

Additional fixed points for Eq. (3) can exist depending on the parameter values. Specifically, since $\lim_{v\to\infty}p(v)=-\infty$ and $p(0)=-c^3$, it follows that, including repeated roots, p can either have zero or two positive roots. Consequently, this system can exhibit a saddle–node bifurcation in which a stable node S (stable storm state) and a saddle V (unstable storm state) emerge or disappear when varying a parameter; see Fig. 2(a) for an example bifurcation diagram in the parameter c. The saddle–node bifurcation occurs when the local maximum v^* of p(v) intersects the v-axis, i.e., $p(v^*)=0$. Calculating v^* we find

$$v^* = \frac{-c + \sqrt{\frac{1}{3}(1 - \gamma)^2 + c^2\gamma}}{1 - \gamma},\tag{5}$$

and thus as functions of c and γ the curve along which the bifurcations occur are given as the 0-level curve of $p(v^*)$. In Fig. 2(b) we plot a "phase diagram" in which the 0-level curve of $p(v^*)$ partitions the (c,γ) plane into regions in which a stable storm state does (labeled Existence of Storm State) or does not exist (labeled Existence of Non-Storm State).

Fig. 2(a) and (c) indicate that for $c \ll 1$, \mathcal{U} remains close to the origin while the v-coordinate of \mathcal{S} varies linearly in c. This result can be verified by an asymptotic expansion of the zeros of p(v). Specifically, we assume an asymptotic expansion of a fixed point (v^*, m^*) in the form

$$v^* = v_0 + c^{\alpha_1} v_1 + c^{\alpha_2} v_2 + \cdots,$$

$$m^* = \frac{v^*}{v^* + c},$$
(6)

where $0<\alpha_1<\alpha_2<\cdots$. At lowest order in c we obtain the cubic equation $v_0(1-\gamma)(1-v_0)^2=0$ and thus the non-negative roots are $v_0=0$ and $v_0=1$ which correspond to the lowest order approximations of $\mathcal U$ and $\mathcal S$ respectively.

1. If we continue the expansion assuming $v_0=0$, we find that to balance terms we need $\alpha_1=3,\alpha_2=5,\ v_1=(1-\gamma)^{-1},\ v_2=3(1-\gamma)^{-2}$ and therefore

$$m^* = \frac{c^3 (1 - \gamma)^{-1} + 3c^5 (1 - \gamma)^{-2} + \dots}{c + c^3 (1 - \gamma)^{-1} + 3c^5 (1 - \gamma)^{-2} + \dots} = \frac{c^2}{1 - \gamma} + \frac{2c^4}{(1 - \gamma)^2} + \dots$$
 (7)

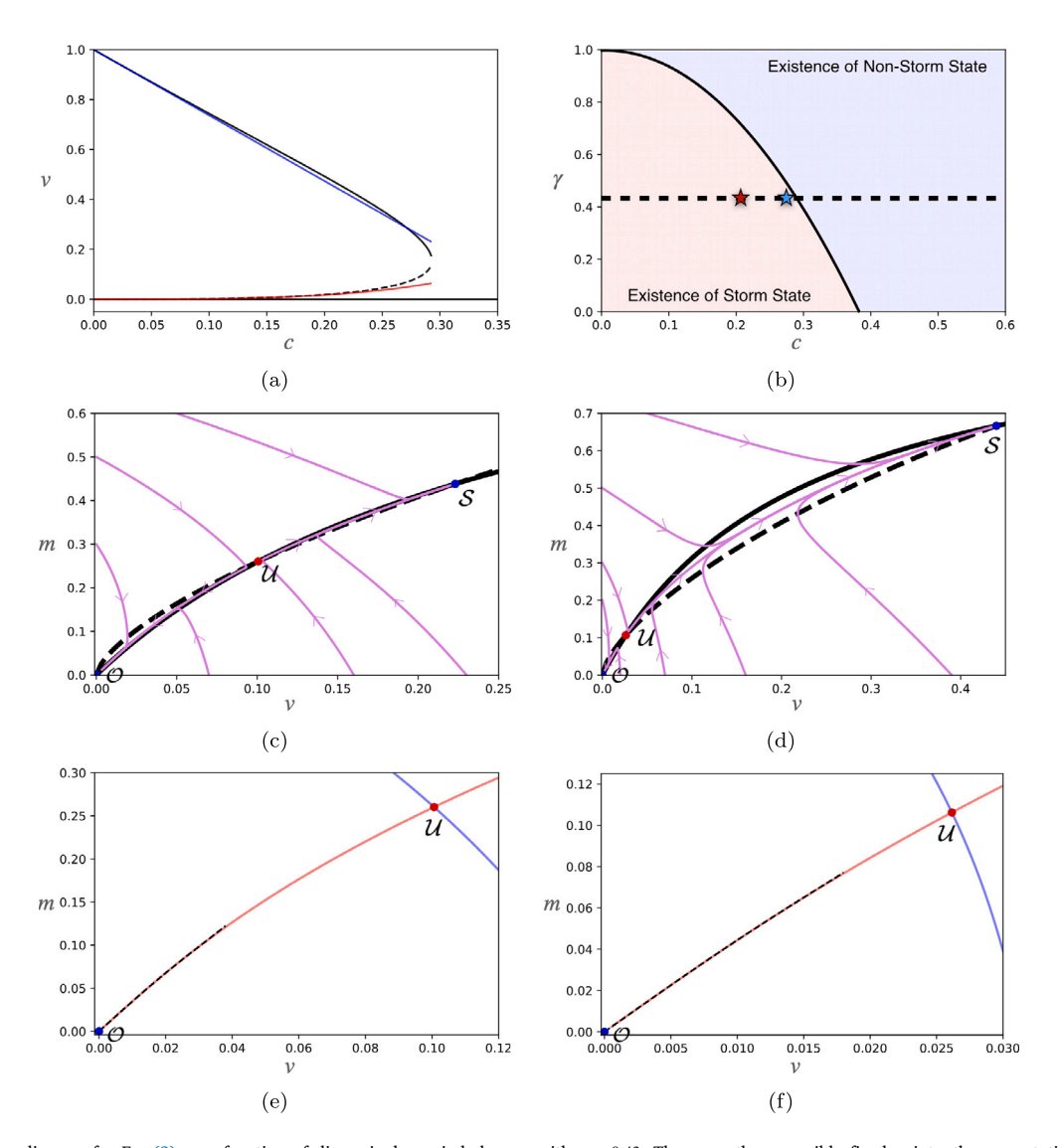


Fig. 2. (a) Bifurcation diagram for Eq. (3) as a function of dimensionless wind shear c with $\gamma=0.43$. There are three possible fixed points: the asymptotically stable origin \mathcal{O} (non-storm state), another asymptotically stable fixed point S (stable storm state), and a saddle \mathcal{U} (unstable storm state). The blue and red curves are the approximations of Eq. (9) for S and \mathcal{U} , respectively. (b) Phase diagram for Eq. (3) in the (γ,c) plane in which the regions corresponding to the existence or non-existence of S and \mathcal{U} are labeled as Existence of Storm State and Non-Storm State respectively. (c-d) Phase portraits for Eq. (3) with $(\gamma,c)=(0.43,0.286)$ (blue star in (b)) and $(\gamma,c)=(0.43,0.22)$ (red star in (b)) respectively. The blue circles correspond to the stable fixed points S and \mathcal{O} and the red circle corresponds to the saddle node \mathcal{U} . The dashed and solid black lines correspond to the nullclines $\dot{v}=0$ and $\dot{m}=0$ respectively. (e-f) Magnifications of the phase portraits in Fig. 2(c-d) near the origin. The red (blue) lines correspond to the unstable (stable) manifold of \mathcal{U} and the dashed line is the local approximation of the center manifold near the origin.

2. Assuming $v_0=1$ we obtain a regular perturbation, i.e., $\alpha_1=1,\alpha_2=2,...$, implying $v_1=-\frac{3}{2}(1-\gamma)^{-1},\ v_2=-\frac{3}{8}(1-4\gamma)(1-\gamma)^{-2}$ and thus

$$m^* = \frac{1 - \frac{3}{2}(1 - \gamma)^{-1}c + \dots}{1 - \left(\frac{3}{2}(1 - \gamma)^{-1}c - c\right)} = 1 - c + \dots.$$
 (8)

Therefore, the first two nonzero terms in the asymptotic expansions for $\mathcal U$ and $\mathcal S$ in c are given by

$$\mathcal{U} = \left(\frac{c^3}{1 - \gamma} + \frac{3c^5}{(1 - \gamma)^2}, \frac{c^2}{1 - \gamma} + \frac{2c^4}{(1 - \gamma)^2}\right) + \left(o(c^5), o(c^4)\right),
S = \left(1 - \frac{3}{2}(1 - \gamma)c, 1 - c\right) + \left(o(c^2), o(c^2)\right).$$
(9)

The asymptotic expansion in Eq. (9) indicates that for weak wind shear the separation in phase space between the non-storm state \mathcal{O} and the unstable storm state \mathcal{U} is small in comparison with the separation between \mathcal{U} and the stable storm state \mathcal{S} . This separation is illustrated by the generic phase portraits of Eq. (3) presented in Fig. 2(c-d) for

parameter values in which S exists. To indicate the basins of attraction for \mathcal{O} and S, denoted $\mathbb{B}(\mathcal{O})$ and $\mathbb{B}(S)$ respectively, in Fig. 2(e-f) we plot the unstable and stable manifolds of \mathcal{U} near the origin. As it will be important in Section 4 when we discuss noise-induced tipping, note that the stable manifold of \mathcal{U} forms a separatrix between $\mathbb{B}(\mathcal{O})$ and $\mathbb{B}(S)$.

A final feature of this dynamical system is the existence of a center manifold near $\mathcal O$ which is approximated to cubic order by

$$m(v) = -\frac{1}{c}v - \frac{1-\gamma}{c^5}v^3; \tag{10}$$

see Appendix A for the derivation. This approximation is overlaid as a dashed curve in Fig. 2(e-f). This manifold acts as a slow manifold near $\mathcal O$ in the sense that, near $\mathcal O$, the component of the vector field transverse to the manifold is much larger in magnitude than the component tangent to the manifold. Consequently, the center manifold provides a natural pathway for noise-induced transitions from $\mathcal O$ to $\mathcal S$ to occur; a conjecture we will verify in Section 4.

3. Rate-induced tipping in the tropical cyclone model

Of central interest is the possibility of transitions between the two stable states as the max potential velocity, V_p , and the dimensionless wind shear, c, vary in time. While the analysis used to study both bifurcation and noise-induced tipping relies on small c, rate-induced tipping does not need to assume anything particular about the size of c. Rate-induced tipping is where a sufficiently quick change to a parameter of a system may cause the system to move away from one attractor to another, without undergoing a bifurcation [1]. Essentially, the system is unable to track a continuously changing attractor if the parameter changes fast enough.

3.1. A quick introduction to rate-induced tipping

Following the work of [1,22], we lay out the framework needed to describe rate-induced tipping and introduce the necessary notation.

Consider the autonomous differential equation

$$\dot{x} = f(x, \lambda),\tag{11}$$

where $x \in \mathbb{R}^n, \lambda \in \mathbb{R}^m, f \in C^2(\mathbb{R}^{m+n}, \mathbb{R}^n), t \in \mathbb{R}$, and $\dot{x} = \frac{dx}{dt}$. Now, instead of a fixed λ , suppose that λ changes in time. We replace λ with an external input $\Lambda_r(t) = \Lambda(rt) \in C^2(\mathbb{R}, \mathbb{R}^m), \ r \geq 0$, and specifically assume that Λ_r is bi-asymptotically constant. In other words, Λ_r is a parameter shift that satisfies

$$\lim_{t \to -\infty} \Lambda_r(t) = \lambda^- \in \mathbb{R}^m \text{ and } \lim_{t \to \infty} \Lambda_r(t) = \lambda^+ \in \mathbb{R}^m, \tag{12}$$

where λ^- is the past limit state and λ^+ is the future limit state. In addition to assuming that Λ_r is bi-asymptotically constant, assume that Λ_r is monotonically increasing, and that $\lambda^- < \Lambda_r < \lambda^+$. These assumptions on Λ_r allow a transition between λ^- and λ^+ in time, where the size of r, the rate parameter, determines how quickly Λ_r transitions between λ^- and λ^+ . While there are different types of functions that fit these criteria, we use a transformed hyperbolic tangent function as Λ_r . Note that the external input Λ_r is often called a ramp function or a ramp parameter.

With $\lambda = \Lambda_r(t) = \Lambda(rt)$, Eq. (11) becomes

$$\dot{x} = f(x, \Lambda_r(t)),\tag{13}$$

where r is any non-negative real number. Since this is a non-autonomous system, it is natural to introduce an auxiliary variable s = rt and $\Lambda(s) = \Lambda(rt)$, and rewrite Eq. (11) as

$$\dot{x} = f(x, \Lambda(s)),
\dot{s} = r.$$
(14)

Alternatively, to convert the nonautonomous system into an autonomous system, we could use *compactification* [42]. In this process, the invertibility of the time-dependent parameter is used to make a coordinate transform and then the system is augmented into an autonomous n+1-dimensional extended system. The compactified system will contain equilibria and compact invariant sets in the extended phase space, such as unstable and stable manifolds, allowing us to use tools and methods from dynamical systems to study the compactified system. Solutions of Eq. (13) that remain bounded as $t \to \pm \infty$ become heteroclinic connections in the compactified system [42]. Therefore, compactification allows for the analysis of nonautonomous rate-induced tipping in finite phase space. Using $y = \Lambda_r(t)$ as an additional dependent variable, and based on the assumptions of $\Lambda_r(t)$, y is invertible. Due to this invertibility of y, the differentiation and substitution results in the first order system given by

$$\dot{x} = f(x, \Lambda_r(\Lambda_r^{-1}(y))) = f(x, y),
\dot{y} = \dot{\Lambda}_r(\Lambda_r^{-1}(y)).$$
(15)

We will continue to use the setup as given in Eq. (14), but we illustrate both systems' behaviors in Fig. 3.

Definition 3.1. Suppose that $\Lambda(s)$ satisfies Eq. (12), and that for all $s \in \mathbb{R}$, X(s) is a fixed point of Eq. (11) when $\lambda = \Lambda(s)$, where s is viewed as a parameter, or equivalently, (X(s), s) is a fixed point of Eq. (14) for each s with r = 0. If (X(s), s) is a connected curve, then we call (X(s), s) a *stable (unstable) path* if X(s) is an attracting (repelling) fixed point of Eq. (11), with $\lambda = \Lambda(s)$ for each fixed s.

Using this definition, we can say when rate-induced tipping occurs away from a stable path. We consider (stable) paths that tend to fixed stable states of the asymptotic systems at $\pm \infty$. Assume that X(s) = X(rt) is a stable path and that $X(s) \to X^{\pm}$ as $s \to \pm \infty$, where X^{\pm} are attracting states of the asymptotic systems found by replacing, respectively, λ^{\pm} in Eq. (11).

From Theorem 2.2 of [22], there is a unique trajectory of Eq. (13), $x^r(t)$, for which $x^r(t) \to X^-$ as $t \to -\infty$, which is the local pullback attractor associated with X^- . If $x^r(t) \to X^+$, then we say that $x^r(t)$ endpoint tracks the stable path X(s). Note that this will happen if r > 0 is sufficiently small, as shown in Lemma 2.3 of [22]. We can now define when rate-induced tipping occurs.

Definition 3.2. Under the conditions just stated, we say that Eq. (13) undergoes *rate-induced tipping* from X^- if there is a rate r>0 such that $\lim_{t\to\infty} x^r(t) \not\to X^+$. The smallest positive value of r such that $\lim_{t\to\infty} x^r(t) \not\to X^+$ is called the critical rate and is denoted by r_c .

Definition 3.3. Suppose that, for fixed λ , Eq. (11) has a hyperbolic sink X. We define the basin of attraction for X as

 $\mathbb{B}(X,\lambda) =$

 $\{y|x(t) \text{ is a trajectory of Eq. (11) with } x(0) = y \text{ and } \lim_{t \to \infty} x(t) = X\}.$

Essentially, if $r < r_c$, solutions will end-point track the path of fixed points in the frozen time system they were initialized on. However, when $r = r_c$, tipping to the basin boundary of X^- has occurred, and when $r > r_c$, it either tips to infinity or a different attractor. It is worth mentioning that not all choices of Λ_r result in rate-induced tipping. There is theory to let us know if a system will or will not tip with a chosen Λ_r , and the conditions change based on the dimension of the system. Nevertheless, the conditions for a system to undergo rate-induced tipping are the same for arbitrary dimension. In particular, rate-induced tipping can occur in the system given by Eq. (13) if the starting base state satisfies a sufficient condition called *forward threshold unstable* when the parameter shift is applied to it [27]. Condensing the results of the work by [1,43], the following theorem is relevant for the analysis in this section.

Theorem 3.4. Suppose $\Lambda(s)$ gives rise to a stable path (X(s), s) for Eq. (14) with $x \in \mathbb{R}^n$, for $n \ge 1$. As above, when $\lambda = \lambda^{\pm}$, in Eq. (14) the limits of the stable path are stable equilibria in their respective systems and denoted X^{\pm} . If there is a $Y^+ \ne X^+$ such that Y^+ is an attracting equilibrium of Eq. (11) for $\lambda = \lambda^+$, and $X^- \in \mathbb{B}(Y^+, \lambda^+)$, then there is rate-induced tipping away from X^- to Y^+ for this $\Lambda(s)$, for sufficiently large r > 0.

We demonstrate the notions of Definitions 3.1–3.3, and Theorem 3.4 in one-dimension in Fig. 3. Forward threshold stability is not a necessary condition to prevent rate-induced tipping in systems of dimension higher than one. However in [43], it was proposed that the condition of inflowing stability guarantees that rate-induced tipping cannot happen away from a stable path. It is the approach we take to study rate-induced tipping in the tropical cyclone model.

Definition 3.5. Suppose $\Lambda(s)$ gives rise to a stable path (X(s), s) with limiting states X^{\pm} . We say the stable path (X(s), s) is forward inflowing stable if for each $s \in \mathbb{R}$ there is a compact set K(s) such that

- 1. For all $s \in \mathbb{R}$, $X(s) \in \text{Int } K(s)$;
- 2. If $s_1 < s_2$, then $K(s_1) \subset K(s_2)$;
- 3. If $x \in \partial K(s)$, then there is a $t_0 > 0$ so that for all $t \in (0, t_0)$, $x^r(t) \in$ Int K(s) where s = rt;

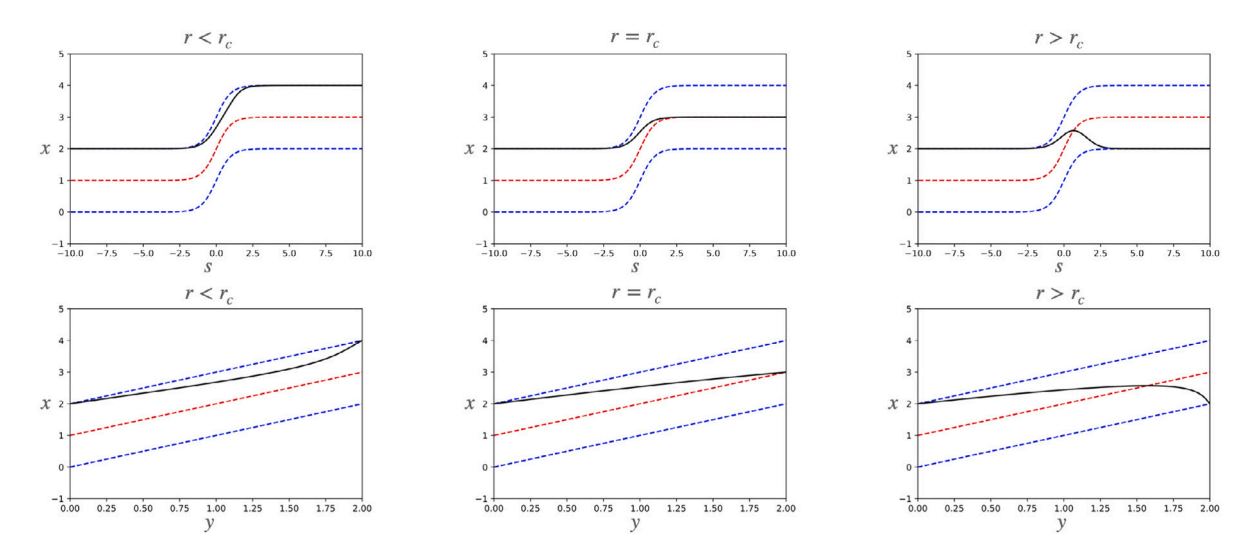


Fig. 3. Consider the system $\dot{x} = -(x - \lambda)(x - \lambda - 1)(x - \lambda - 2)$, where we replace λ with a time-changing parameter $\Lambda_r(t) = 1 + \tanh(rt)$. Notice there are three fixed points: $x = \lambda, \lambda + 1$, and $\lambda + 2$, where $x = \lambda, \lambda + 2$ are stable and $x = \lambda + 1$ is unstable. Solutions (black) are shown for varying values of r. The top row of the figure shows the behavior of Eq. (14) and the bottom row of the figure shows the behavior of Eq. (15). Blue dashed curves track the stable paths (stable fixed points) in the frozen time system, and the red dashed curve tracks the unstable path (unstable fixed point) in the frozen time system. Notice that $(X^- = 2, \lambda^- = 0) \in \mathbb{B}(Y^+ = 2, \lambda^+ = 2)$, satisfying Theorem 3.4, and implying there is rate-induced tipping away from X^- . Rate-induced tipping occurs for $r \ge r_c$.

4.
$$X^{\pm} \in \text{Int } (K_{\pm}) \text{ where } K^{-} = \bigcap_{t \in \mathbb{R}} K(s) \text{ and } K^{+} = \overline{\bigcup_{s \in \mathbb{R}} K(s)};$$

5. $K^{+} \subset B(X^{+}, \lambda^{+}) \text{ is compact.}$

Theorem 3.6. Suppose $\Lambda(s)$ gives rise to a stable path (X(s), s) with asymptotic states X^{\pm} . If it is forward inflowing stable, then there is no rate-induced tipping away from X^- for this $\Lambda(s)$ for any r > 0.

3.2. Necessary conditions for rate-induced tipping in the tropical cyclone model

Using the above framework, we consider the possibility of rate-induced tipping to aid in the destabilization or the formation of a storm by allowing c and V_p to vary with time, as physically, both wind shear and max potential velocity are components of the model that have the ability to change quickly.

We redefine both c and V_p as functions of some parameter shift Λ_r : $\mathbb{R} \to \mathbb{R}$ that varies at a rate r>0, and satisfies the conditions described in Section 3.1. Allowing V_p and c to be dependent on $\Lambda_r(s)$ implies they will ramp between V_p^- to V_p^+ and c^- to c^+ in time, respectively. Therefore, we adjust the nondimensionalization using $\tau=C_d/(2h)V_p^-t$ and $v=V/V_p^-$, instead of V_p , as this parameter is now time dependent. We choose the minimum max storm potential, V_p^- , as the fixed value of $V_p(\tau)$. This change results in Eq. (2) becoming

$$\frac{dv}{d\tau} = \frac{(1-\gamma)V_p(\tau)^2}{V_p^{-2}} m^3 - (1-\gamma m^3)v^2,$$

$$\frac{dm}{d\tau} = (1-m)v - c(\tau)m.$$
(16)

Proposition 3.7. There is no rate-induced tipping away from \mathcal{O} regardless of the Λ_r chosen.

Proof. For all values of c and V_p , $\mathcal O$ is a stable fixed point and $\dot v=\dot m=0$. Therefore, there can be no rate-induced tipping away from $\mathcal O$ for any ramp Λ_r . \square

We will generally assume the values of c and V_p are such that there are three fixed points of Eq. (16) for all values of $\Lambda_r(\tau)$, as this is the most interesting case to study due to Proposition 3.7. However, we describe the other cases and their outcomes below.

Case 1. Assume that the values of c and V_p are chosen so there is only one fixed point of Eq. (16) when $\Lambda_r(\tau) = \lambda^-$, and one or three fixed

points of Eq. (16) when $\Lambda_r(\tau) = \lambda^+$. If there is only one fixed point when $\Lambda_r(\tau) = \lambda^-$, it has to be the origin, \mathcal{O} , as shown in the deterministic analysis conducted in Section 2. By Proposition 3.7, there can be no rate-induced tipping away from \mathcal{O} .

Case 2. Assume that the values of c and V_p are chosen so there are three fixed points of Eq. (16) when $\Lambda_r(\tau) = \lambda^-$, \mathcal{O} , \mathcal{U}^- , \mathcal{S}^- , and one fixed point of Eq. (16) when $\Lambda_r(\tau) = \lambda^+$. The fixed point when $\Lambda_r(\tau) = \lambda^+$ must be the origin by the deterministic analysis conducted in Section 2. By Proposition 3.7, there will be no rate-induced tipping away from \mathcal{O} . If we look at tipping away from \mathcal{S}^- , we have to tip to \mathcal{O} , independent of r, undergoing bifurcation tipping, as we have the annihilation of two fixed points.

The case we will exemplify is when we assume that the values of c and V_p are chosen such that there are three fixed points of Eq. (16) when $\Lambda_r(\tau) = \lambda^- : \mathcal{O}, \mathcal{V}^-, S^-$ and three fixed points of Eq. (16) when $\Lambda_r(\tau) = \lambda^+ : \mathcal{O}, \mathcal{V}^+, S^+$. We will make use of Proposition 3.8 within the proof of Theorem 3.9. See Appendix C for the proof of this proposition. We reintroduce the polynomial in Eq. (4) to include V_p . Let

$$p_{new}(v, V_p, c) = (1 - \gamma) \frac{V_p}{V_p^-} v + \gamma v^3 - (v + c)^3.$$
 (17)

Proposition 3.8. Suppose V_p , c > 0 such that $p_{new}(v, V_p, c)$ has two positive zeros, $0 < v_1 < v_2$. If $a = (a_1, a_2)$ and $b = (b_1, b_2)$ satisfy

$$\begin{cases} v_1 < a_1 < v_2 \\ \sqrt[3]{\frac{a_1^2}{(1-\gamma)(\frac{V_p}{V_p^*})^2 + \gamma a_1^2}} < a_2 < \frac{a_1}{a_1 + c} \end{cases} \quad and \quad \begin{cases} v_2 < b_1 \\ \frac{b_1}{b_1 + c} < b_2 < \sqrt[3]{\frac{b_1^2}{(1-\gamma)(\frac{V_p}{V_p^*})^2 + \gamma b_1^2}} \end{cases}$$

then the box $K_{a,b} = [a_1, b_1] \times [a_2, b_2]$ is forward invariant with respect to the flow.

Theorem 3.9. Assume that $\Lambda_r(\tau), V_p(\Lambda_r(\tau))$, and $c(\Lambda_r(\tau))$ are chosen such that there are three fixed points at $\Lambda_r(\tau) = \lambda^- : \mathcal{O}, \mathcal{U}^-, S^-$ and three fixed points at $\Lambda_r(\tau) = \lambda^+ : \mathcal{O}, \mathcal{U}^+, S^+$. Assume that there exist paths $(\tau, p_u(\tau))$ and $(\tau, p_s(\tau))$ and they are distinct for all values of τ . If either $V_p(\Lambda_r(\tau))$ or $c(\Lambda_r(\tau))$ is nonincreasing as a function of τ , there can be no rate-induced tipping away from the stable storm state S^- to the non-storm state \mathcal{O} .

Proof. We will prove that if either $V_p(\Lambda_r(\tau))$ or $c(\Lambda_r(\tau))$ is nonincreasing as a function of τ , then $(\tau, p_s(\tau))$ is forward inflowing stable and hence there can be no rate-induced tipping away from \mathcal{S}^- .

First suppose $V_p(\Lambda_r(\tau))$ is nonincreasing. Write $p_s(\tau)=(v_2(\tau),m_2(\tau))$. For each value of V_p there is a unique value of c, call it $c^*(V_p)$ for which there is exactly one positive zero of polynomial p_{new} , in Eq. (17). Since $p_{new}(v,V_p,c^*(V_p))=0$ if and only if $p_{new}(\epsilon v,\epsilon V_p,\epsilon c^*(V_p))=0$ for any $\epsilon>0$, it follows that $c^*(\epsilon V_p)=\epsilon c^*(V_p)$. If we let $v^*(V_p)$ denote the unique zero of $p_{new}(v,V_p,c^*(V_p))$ then also $v^*(\epsilon V_p)=\epsilon v^*(V_p)$. In particular, v^* is strictly increasing as a function of V_p . If we let $m^*(V_p)=\frac{v^*(V_p)}{v^*(V_p)+c^*(V_p)}$ then $m^*(\epsilon V_p)=m^*(V_p)$ for all $\epsilon>0$, and we can call this common value m^*

Now we would like to find functions $a_1, a_2 : \mathbb{R} \to \mathbb{R}$ that satisfy

$$\begin{cases} v^*(V_p(\Lambda_r(\tau))) & < a_1(\tau) < & v_2(\tau) \\ m^* & < a_2(\tau) < & \frac{a_1(\tau)}{a_1(\tau) + c(\Lambda_r(\tau))} \end{cases}$$
 (18)

for all $\tau \in \mathbb{R}$. It is possible to find these functions a_1, a_2 by the following argument. For any value of s, we may assume $c(\Lambda_r) \in (0, c^*(V_p(\Lambda_r)))$ since we are assuming the paths $(\tau, p_u(\tau))$ and $(\tau, p_s(\tau))$ exist and are distinct. This implies $v^*(V_p(\Lambda_r(\tau))) < v_2(\tau)$ and so we can choose $a_1(\tau)$ to satisfy the first inequality. Given this,

$$m^* = \frac{v^*(V_p(\Lambda_r(\tau)))}{v^*(V_p(\Lambda_r(\tau))) + c^*(V_p(\Lambda_r(\tau)))} < \frac{v^*(V_p(\Lambda_r(\tau)))}{v^*(V_p(\Lambda_r(\tau))) + c(\Lambda_r(\tau))} < \frac{a_1(\tau)}{a_1(\tau) + c(\Lambda_r(\tau))},$$
(19)

and so we can choose $a_2(\tau)$ to satisfy the second inequality. Furthermore, we would like to enforce a_1, a_2 be continuous and nonincreasing, which is possible since $v^*(V_\rho(\Lambda_r(\tau)))$ and m^* are both nonincreasing.

Also pick constants b_1, b_2 such that

$$\begin{cases} v_2(\tau) & < b_1 \\ \frac{b_1}{b_1 + c(\Lambda_r(\tau))} & < b_2 < \sqrt[3]{\frac{b_1^2}{(1 - \gamma)(\frac{V_p(\Lambda_r(\tau))}{V_-})^2 + \gamma b_1^2}} \end{cases}$$
 (20)

for all τ . For each τ define $K(\tau) = [a_1(\tau),b_1] \times [a_2(\tau),b_2]$. By Proposition 3.8, each $K(\tau)$ is forward invariant with respect to the flow when $V_p = V_p(\Lambda_r(\tau))$ and $c = c(\Lambda_r(\tau))$. By how we defined $\{K(\tau)\}$, they satisfy Definition 3.5 to show $(\tau,p_s(\tau))$ is forward inflowing stable path and so there can be no rate-induced tipping away from S^- .

Next suppose $c(\Lambda_r(\tau))$ is nonincreasing. For each value of c there is a unique value of V_p , call it $V_p^*(c)$ for which there is exactly one positive zero of the polynomial p_{new} , in Eq. (17). Since $p_{new}(v,V_p^*(c),c)=0$ if and only if $p_{new}(\epsilon v,\epsilon V_p^*(c),\epsilon c)=0$ for any $\epsilon>0$, it follows that $V_p^*(\epsilon c)=\epsilon V_p^*(c)$. If we let $v^*(c)$ denote the unique zero of $p_{new}(v,V_p^*(c),c)$, then also $v^*(\epsilon c)=\epsilon v^*(c)$. In particular, v^* is strictly increasing as a function of c. If we let $m^*(c)=\frac{v^*(c)}{v^*(c)+c}$, then $m^*(\epsilon c)=m^*(c)$ for all $\epsilon>0$, and we can call this common value m^* .

Now we would like to find continuous nonincreasing functions $a_1,a_2:\mathbb{R}\to\mathbb{R}$ that satisfy

$$\begin{cases} v^*(c(\Lambda_r(\tau))) & < a_1(\tau) < & v_2(\tau) \\ m^* & < a_2(\tau) < & \frac{a_1(\tau)}{a_1(\tau) + c(\Lambda_r(\tau))} \end{cases}$$
 (21)

for all $\tau \in \mathbb{R}$. The reasons for why this is possible are the same as those described earlier in this argument. Also, pick constants b_1,b_2 to satisfy Eq. (20) for all τ . Then define $K(\tau) = [a_1(\tau),b_1] \times [a_2(\tau),b_2]$. Once again, these sets can be used to show that $(\tau,p_s(\tau))$ is a forward inflowing stable path. Therefore there can be no R-tipping away from \mathcal{S}^- . \square

Interestingly, if both $V_p(\Lambda_r(\tau))$, and $c(\Lambda_r(\tau))$ are increasing, then Theorem 3.9 allows for the possibility of rate-induced tipping from S^- to \mathcal{O} for $r>r_c$, as the example in Section 3.3 will demonstrate. Fig. 4(b) highlights both solutions that do not tip $(r< r_c)$ and solutions that do tip $(r>r_c)$. Using the results above, a mathematically general form of our ramped parameters V_p and c that will result in rate-induced tipping for $r>r_c$ is given by

$$\begin{split} V_p(\tau) &= V_p^-(1-\Lambda_r(\tau)) + V_p^+\Lambda_r(\tau), \\ c(\tau) &= kV_p(\tau), \end{split} \tag{22}$$

where k is a correlation coefficient between V_p and c, and the functions Λ_r, V_p , and c are chosen such that three fixed points, two stable and one saddle, exist for all time.

3.3. Example of rate-induced tipping in the tropical cyclone model

As the problem we investigate in this analysis is in \mathbb{R}^2 , we must understand the basin of attraction in two-dimensional space. For both $\Lambda_r(\tau) = \lambda^-$ and $\Lambda_r(\tau) = \lambda^+$, we have two asymptotically stable fixed points that are separated by a saddle node, whose stable manifold forms a separatrix for the basins of attraction of $\mathcal O$ and $\mathcal S^-$ and $\mathcal O$ and $\mathcal S^+$ respectively. If $\mathcal S^- \in \mathbb B(\mathcal O, \lambda^+)$, we will have rate-induced tipping away from $\mathcal S^-$ by Theorem 3.4.

Using what we learned in Section 3.2, we choose a parameter shift $\Lambda_r(\tau)$, and increasing functions V_p and c that are dependent on $\Lambda_r(\tau)$ such that $S^- \in \mathbb{B}(\mathcal{O}, \lambda^+)$. One such choice is

$$\Lambda_r(\tau) = \frac{1}{2}(1 + \tanh(r\tau)),\tag{23}$$

$$V_p(\tau) = 90\Lambda_r(\tau) + 10,$$
 (24)

$$c(\tau) = 0.13V_n(\tau),\tag{25}$$

where the ratio between $V_{\rho}(r)$ and c(r) is fixed at 0.13 to guarantee that there are always three equilibria. For this choice in functions, $S^- \in \mathbb{B}(\mathcal{O}, \lambda^+)$, as seen in Fig. 4(a). This indicates by Theorem 3.4 that there will be rate-induced tipping away from S^- to \mathcal{O} for sufficiently large r>0. We choose a c value to satisfy this theorem as in dimensions n>1, $X^-\notin \mathbb{B}(Y^+,\lambda^+)$ does not necessarily prevent tipping from occurring. The ratio is chosen to guarantee rate-induced tipping, but we note that other c values provide similar results.

Using our approach from Section 3.1 to convert Eq. (16) back to an autonomous system, we have the system of first order equations given by

$$\frac{dv}{d\tau} = \frac{(1 - \gamma)V_p(s)^2}{V_p^{-2}} m^3 - (1 - \gamma m^3)v^2,
\frac{dm}{d\tau} = (1 - m)v - c(s)m,
\frac{ds}{d\tau} = 1.$$
(26)

Solving this system, we determine for $r < r_c$ we endpoint track the stable path from S^- to S^+ . However, when $r > r_c$ we tip from S^- to \mathcal{O} . For $r = r_c$ we have a heteroclinic connection between S^- and \mathcal{U}^+ . Via numerical simulations we find that $r_c \in (0.0506279, 0.050628)$. We show numerical results of tipping in (v, m) space in Fig. 4(b).

In conclusion, we see that due to the stability of the non-storm state, \mathcal{O} , we cannot form a tropical cyclone, but a storm can destabilize with rapidly increasing max potential velocity and dimensionless wind shear.

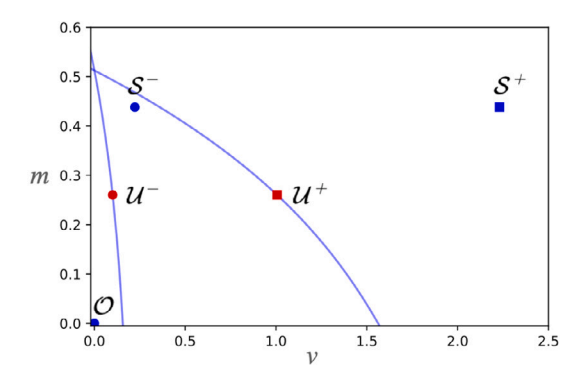
4. Noise-induced tipping in the tropical cyclone model

In this section we study noise-induced transitions between the stable states $\mathcal O$ and $\mathcal S$ for the stochastic differential equation

$$dv = f(v, m)d\tau + \sigma_1 dW_1,$$

$$dm = g(v, m)d\tau + \sigma_2 dW_2,$$
(27)

where $\sigma_1, \sigma_2 > 0$, W_1, W_2 are independent Brownian motions, f, g are defined as in Eq. (3) and in this section we are returning to the dimensionless coordinates introduced in Section 2. In Section 2 we showed that for small wind shear the separation between $\mathcal O$ and $\mathcal V$ is relatively small in comparison with the separation between $\mathcal V$ and $\mathcal S$. Consequently, we expect $\mathcal O$ is highly susceptible to noise-induced tipping while $\mathcal S$ is more robust to random fluctuations. Moreover, the existence of a one-dimensional center manifold near $\mathcal O$ indicates that the deterministic flow is comparatively weak when restricted to this



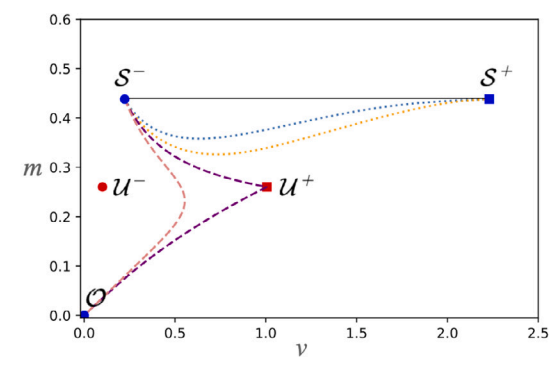


Fig. 4. In both plots the fixed points of the system given by Eq. (3) at the start and end of the ramp function, Eq. (23), are shown. V_p and c, defined by Eqs. (24) and (25), are time dependent and $\gamma=0.43$. The three fixed points at the start of the ramp, $\mathcal{O}, \mathcal{U}^-, S^-$, correspond to the non-storm state, the unstable storm state, and the stable storm state. These stable fixed points are denoted by blue circles and the saddle node is denoted by a red circle. The three fixed points at the end of the ramp, $\mathcal{O}, \mathcal{U}^+, S^+$, correspond to the non-storm state, the unstable storm state, and the stable storm state. These stable fixed points are denoted by blue squares and the saddle is denoted by a red square. (a) Blue curves correspond to the stable manifolds of \mathcal{U}^- and \mathcal{U}^+ . (b) Plot of the solutions to the system given by Eq. (3) for different values or r. The black curve is the solution r=0 and end-point tracks the stable path from S^- to S^+ . The purple (pink) dashed curve corresponds to the solution for r=0.050628 (r=0.08), which do not endpoint track the stable path, and tip from S^- to \mathcal{O} .

manifold, providing a natural region in phase space that is susceptible to noise-induced transitions.

Recall from Section 2 that for physical reasons $v,m\geq 0$ and additionally it can be shown that the autonomous system extended to \mathbb{R}^2 is unstable for v<0 but the first quadrant is invariant. However, since realizations of Eq. (27) can enter these nonphysical regions of phase space, we interpret Eq. (27) to have reflecting boundary conditions along the lines v=0 and m=0. That is, for $(\hat{v},\hat{m})\in\mathbb{R}^2$ we consider the system

$$\begin{split} d\hat{v} &= \hat{f}(\hat{v}, \hat{m}) d\tau + \sigma_1 dW_1, \\ d\hat{m} &= \hat{g}(\hat{v}, \hat{m}) d\tau + \sigma_2 dW_2, \end{split} \tag{28}$$

where the reflected components of the vector field are defined by

$$\hat{f}(\hat{v}, \hat{m}) = \begin{cases} f(\hat{v}, \hat{m}) & \hat{v} > 0, \hat{m} > 0 \\ -f(-\hat{v}, \hat{m}) & \hat{v} < 0, \hat{m} > 0 \\ -f(-\hat{v}, -\hat{m}) & \hat{v} < 0, \hat{m} < 0 \end{cases}$$

$$f(\hat{v}, -\hat{m}) & \hat{v} > 0, \hat{m} < 0,$$

$$\hat{g}(\hat{v}, \hat{m}) = \begin{cases} = g(\hat{v}, \hat{m}) & \hat{v} > 0, \hat{m} > 0 \\ -g(-\hat{v}, \hat{m}) & \hat{v} < 0, \hat{m} > 0 \end{cases}$$

$$-g(-\hat{v}, -\hat{m}) & \hat{v} < 0, \hat{m} > 0$$

$$-g(-\hat{v}, -\hat{m}) & \hat{v} < 0, \hat{m} < 0 \end{cases}$$

$$g(\hat{v}, -\hat{m}) & \hat{v} > 0, \hat{m} < 0.$$
(29)

Realizations to Eq. (28) are then mapped to realizations of Eq. (27) with reflecting boundary conditions by setting $(v(\tau), m(\tau)) = (|\hat{v}(\tau)|, |\hat{m}(\tau)|)$; see Fig. 5(a-b). Throughout the rest of this document we will suppress this notation with the understanding that when referring to f, g we are in fact using the reflected components \hat{f}, \hat{g} and when referring to Eq. (27) we are in fact referring to Eq. (28).

To be precise when discussing noise-induced tipping, we provide the following definition.

Definition 4.1. A noise-induced transition from \mathcal{O} to S, or noise-induced tipping event from \mathcal{O} to S, is a realization of Eq. (27) satisfying $(\underline{v}(0), m(0)) = (0, 0)$, and there exists $\tau^* \in \mathbb{R}^+$ for which $(\underline{v}(\tau^*), m(\tau^*)) \in \overline{\mathbb{B}(S)}$ and for $\tau < \tau^*$, $(\underline{v}(\tau), m(\tau)) \in \mathbb{B}(\mathcal{O})$. The variable τ^* is itself a random variable, specifically a stopping time for this process, and is referred to as the tipping time from \mathcal{O} to S.

We note that similar definition holds for noise-induced transitions from $\mathcal S$ to $\mathcal O$ and the corresponding tipping time τ^* from $\mathcal S$ to $\mathcal O$. Moreover, since the noise is additive, it follows that for our system $\mathbb P(\tau^*<\infty)=1$.

In Fig. 5(c-d) and Fig. 5(e) we plot the time series of $m(\tau)$ for realizations of Eq. (27) that start at \mathcal{O} and \mathcal{S} respectively. From these

numerical experiments we can obtain further evidence that \mathcal{O} is far more susceptible to noise-induced tipping than \mathcal{S} . That is, the expected value of the tipping time from \mathcal{O} to \mathcal{S} is dramatically smaller than from \mathcal{S} to \mathcal{O} . Moreover, as seen in Fig. 5, the noise-induced tipping events from \mathcal{O} to \mathcal{S} appear to be concentrated about a particular region in phase space. To validate these numerical observations, we will use the Freidlin–Wentzell theory of large deviations to quantify the most probable noise-induced transitions as well as the expected tipping time.

4.1. A quick introduction to most probable transitions

In this subsection we present the Freidlin–Wentzell theory of large deviations to provide a framework for computing most probable transition paths from $\mathcal O$ to $\mathcal S$ noting that the same theory can be applied to compute most probable transition paths from $\mathcal S$ to $\mathcal O$. This framework is presented in Freidlin and Wentzel's book [30], the review article by Forgoston and Moore [28], and the review article by Berglund [29] (for gradient systems). In particular, Ref. [44] provides a nice introduction to the Freidlin–Wentzell theory of large deviations within the context of a climate application. To simplify the following exposition, we let F = (f,g) denote the vector field with components f and g, introduce the matrix

$$\Sigma = \begin{bmatrix} \sigma_1^{-2} & 0\\ 0 & \sigma_2^{-2} \end{bmatrix},\tag{30}$$

and define for $v_1,v_2\in\mathbb{R}^2$ the weighted inner product $\langle v_1,v_2\rangle_{\varSigma}=v_1^T\varSigma v_2$ and the weighted norm $\|v_2-v_1\|_{\Sigma}^2=\langle v_2-v_1\rangle_{\varSigma}$. We begin with a definition of a most probable path that summarizes and combines the definitions appearing in [29,30,44,45].

Definition 4.2. A curve $\Psi(s) = (\psi_1(s), \psi_2(s))$ is a most probable transition path between \mathcal{O} and S on the domain $[\tau_0, \tau_f]$ if it minimizes the Freidlin–Wentzell rate functional

$$I[\Psi] = \frac{1}{2} \int_{\tau_0}^{\tau_f} \|\dot{\Psi} - F(\Psi)\|_{\Sigma}^2 ds, \tag{31}$$

over the admissible set

$$\mathcal{A}_{\mathcal{O}}^{(\tau_0,\tau_f)} = \{ \Psi \in H^1([\tau_0,\tau_f];\mathbb{R}^2) : \Psi(\tau_0) = \mathcal{O} \text{ and } \Psi(\tau_f) = S \}. \tag{32}$$

The *most probable path* Ψ^* , if it exists, is the minimizer of the double optimization problem

$$\inf_{[\tau_0,\tau_f]} \inf_{\Psi \in \mathcal{A}_{\alpha}^{(\tau_0,\tau_f)}} I[\Psi]. \tag{33}$$

Note, in terms of notation we represent the most probable transition path as $\Psi = (\psi_1(s), \psi_2(s))$ instead of (v(s), m(s)) to distinguish it from

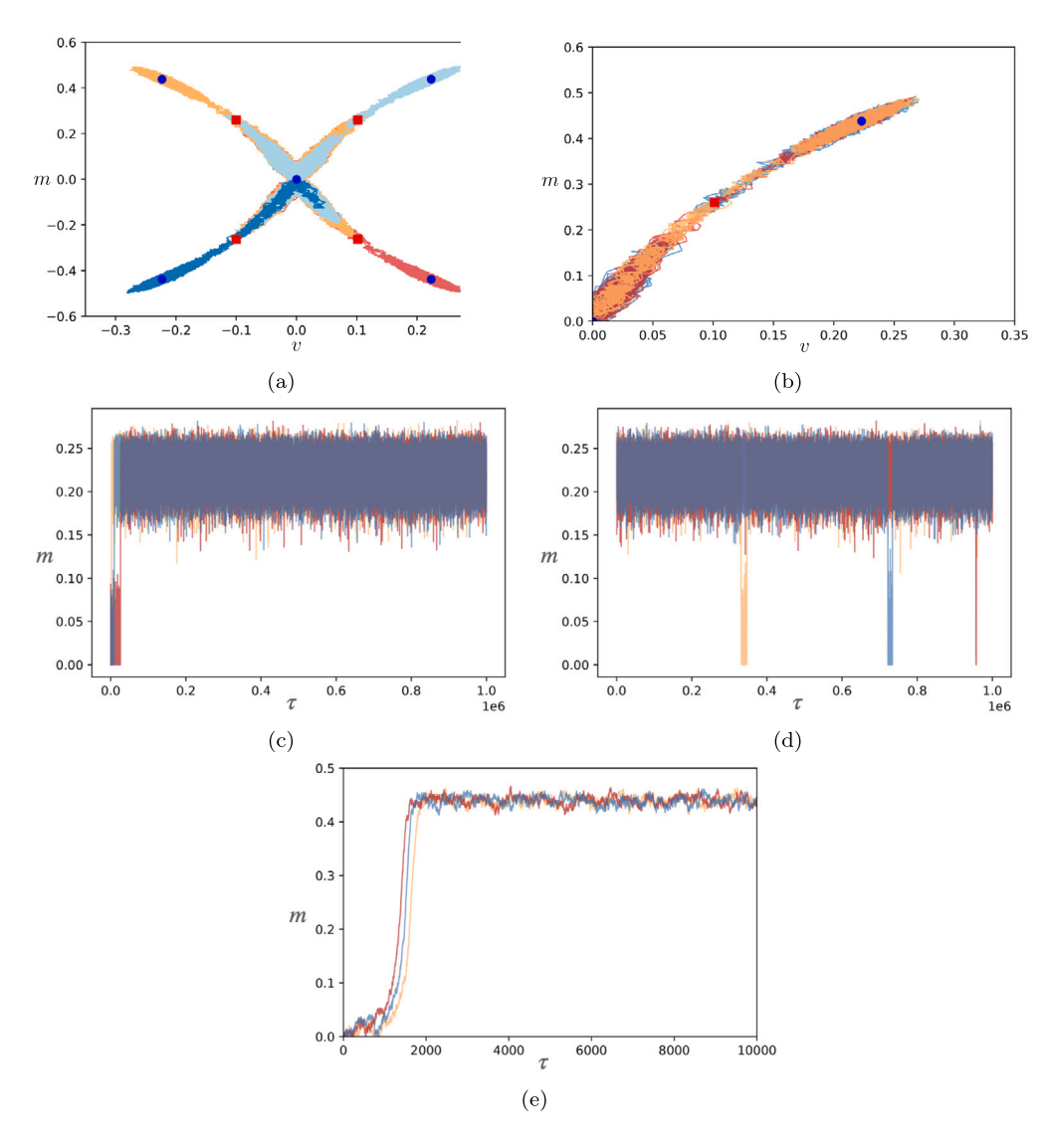


Fig. 5. (a) Realizations of Eq. (28) with $\sigma_1 = \sigma_2 = 0.005$, $\gamma = 0.43$, $V_p = 10$, and c = 0.286. (b) Realizations of Eq. (27) with reflecting boundary conditions, computed by mapping realizations of Eq. (28) to the first quadrant. In both (a-b), stable fixed points for the deterministic dynamics correspond to blue circles while red squares correspond to the saddles. (c-e) Time series of three realizations of Eq. (27) with differing values of c, with $d\tau = 0.1$, and $\tau_f = 10^6$. (c) c = 0.286 with realizations initialized at the non-storm state \mathcal{O} . (d) c = 0.286 with realizations initialized at the stable storm state S. (e) c = 0.22 with realizations initialized at the non-storm \mathcal{O} .

a generic realization of the deterministic dynamics. Additionally, note the functional I as defined above also depends on τ_0, τ_f but we suppress this dependence to simplify notation. Moreover, we will later show that the minimizer over this double optimization can only be obtained when $\tau_0 = -\infty$ and $\tau_f = \infty$.

Summarizing the key concepts in [30], the Freidlin–Wentzell large deviations principle for Eq. (27) states formally that as $\sigma_1,\sigma_2\to 0$ the probability that a realization $(v(\tau),m(\tau))$ of Eq. (27) remains within a $\delta>0$ neighborhood of $\Psi\in\mathcal{A}_{\mathcal{O}}^{(\tau_0,\tau_f)}$ is given by

$$\mathbb{P}\left(\sup_{\tau\in[\tau_0,\tau_f]}\|(v(\tau),m(\tau))-\Psi(\tau)\|<\delta\right)\asymp e^{-I[\Psi]},\tag{34}$$

where \asymp denotes logarithm equivalence. \(^1\) Consequently, in the limit $\sigma_1, \sigma_2 \to 0$, the most probable path Ψ^* can be interpreted as the mode of the probability distribution on $\mathcal{A}_{\mathcal{O}}^{(\tau_0, \tau_f)}$. Additionally, the expected value of the tipping time can be computed from knowledge of the most

probable path by the formula

$$\mathbb{E}[\tau^*] \approx e^{I[\Psi^*]}.\tag{35}$$

Heuristically, Eq. (35) can be justified by letting $p = \exp(-I[\Psi^*])$ approximate the probability of a realization of Eq. (27) leaving $\mathbb{B}(\mathcal{O})$ in an interval of time $[\tau_0, \tau_f]$. In the limit $\sigma_1, \sigma_2 \to 0$ it can be shown that p has approximately a geometric distribution, i.e., the realization either leaves $\mathbb{B}(\mathcal{O})$ or returns to \mathcal{O} in the given interval of time, and thus following this logic $\mathbb{E}[\tau^*] \approx 1/p = \exp(I[\Psi^*])$ [29].

Eq. (34) indicates that the most probable path Ψ^* defined above corresponds to the curve in phase space in which noise-induced transitions from $\mathcal O$ to S concentrate about in the vanishing noise limit $\sigma_1,\sigma_2\to 0$. Moreover, the infimum over $[\tau_0,\tau_f]$ can be interpreted as resulting from accounting for all possible parameterizations of the curve. However, note that I vanishes along curves in which Ψ tracks the deterministic dynamics, i.e., $\dot{\Psi}=F(\Psi)$. Consequently, once Ψ^* crosses the separatrix $\partial\mathbb B(\mathcal O)\cap\partial\mathbb B(S)$, the most probable path Ψ^* will simply satisfy $\dot{\Psi}^*=F(\Psi^*)$ in this region of phase space. Therefore, we can consider the equivalent optimization problem

$$\inf_{[\tau_0,\tau_f]} \inf_{\boldsymbol{\Psi} \in \overline{\mathcal{A}}_0^{(\tau_0,\tau_f)}} I[\boldsymbol{\Psi}],\tag{36}$$

¹ For real sequences x_{ε} , y_{ε} we say $x_{\varepsilon} \asymp y_{\varepsilon}$ if $\lim_{\varepsilon \to 0} \frac{\ln(x_{\varepsilon})}{\ln(y_{\varepsilon})} = 1$.

where

$$\overline{\mathcal{A}}_O^{(\tau_0,\tau_f)} = \{ \Psi \in H^1([\tau_0,\tau_f]; \mathbb{R}^2) : \Psi(\tau_0) = \mathcal{O} \text{ and } \Psi(\tau_f) \in \partial \mathbb{B}(\mathcal{O}) \cap \partial \mathbb{B}(\mathcal{S}) \}.$$
(37)

We can reduce the complexity of this optimization problem by proving that we can take $\tau_f = \infty$ in Eq. (36) by studying the corresponding Euler–Lagrange equations and its natural boundary conditions. Taking the first variation of I over $\mathcal{A}_{\mathcal{O}}^*$ and integrating by parts yields

$$\delta I = \int_{\tau_0}^{\tau_f} \left\langle -\ddot{\Psi} + \nabla F(\Psi)\dot{\Psi} - \Sigma^{-1}\nabla F^T(\Psi)\Sigma(\dot{\Psi} - F(\Psi)), \delta\Psi \right\rangle_{\Sigma} ds + \left\langle \dot{\Psi} - F(\Psi), \delta\Psi \right\rangle_{\Sigma} \Big|_{\tau_f}.$$
(38)

Consequently, the Euler-Lagrange equations are given by

$$\ddot{\Psi} = \nabla F(\Psi)\dot{\Psi} - \Sigma^{-1}\nabla F^{T}(\Psi)\Sigma(\dot{\Psi} - F(\Psi)),\tag{39}$$

with the additional "natural boundary condition" that $\dot{\Psi}(\tau_f) = F(\Psi(\tau_f))$ on the separatrix, i.e., Ψ tracks the flow on the separatrix. Therefore, since the separatrix in this problem corresponds to the stable manifold of $\mathcal U$ and Ψ can track the flow of F at zero cost, it follows that the infimum of (36) is obtained when $\tau_f = \infty$, Ψ^* terminates at $\mathcal S$, and $\lim_{s \to \infty} \dot{\Psi}^*(s) = F(\mathcal S) = 0$.

We now show that we can further reduce the complexity of this problem by assuming $\tau_0=-\infty$. We do this by putting Eq. (39) into Hamiltonian form through the Legendre transform $\mathbf{p}=(p_1,p_2)=\Sigma(\dot{\Psi}-F(\Psi))$ [28]. Through this transformation, we obtain the following Hamiltonian system

$$\dot{\Psi} = F(\Psi) + \Sigma^{-1} \mathbf{p},$$

$$\dot{\mathbf{p}} = -\nabla F^T \mathbf{p},$$
(40)

with corresponding Hamiltonian

$$H = \frac{1}{2} \|\mathbf{p}\|_{\Sigma^{-1}}^2 + \langle F(\Psi), \mathbf{p} \rangle. \tag{41}$$

With this change of variables, the Freidlin–Wentzell rate functional transforms into the following simple form:

$$I[\Psi, \mathbf{p}] = \frac{1}{2} \int_{\tau_0}^{\tau_f} \|\mathbf{p}\|_{\Sigma}^2 ds.$$
 (42)

Since the Hamiltonian is conserved along the flow generated by Eq. (40) and the most probable path satisfies $\lim_{s\to\infty}\dot{\Psi}^*(s)=F(S)=0$, it follows immediately that H=0 on the most probable path Ψ^* . Moreover, since $F(\mathcal{O})=0$ it follows that for the conjugate momentum \mathbf{p}^* corresponding to Ψ^* , $\lim_{\tau\to\tau_0}\mathbf{p}^*(\tau)=0$. That is, (Ψ^*,\mathbf{p}^*) , if it exists, is a heteroclinic connection between $(\mathcal{O},0)$ and $(\mathcal{U},0)$ in this Hamiltonian system and thus $\tau_0=-\infty$.

There are some additional properties of Eq. (40) which will aid our later analysis.

- 1. Eq. (40) contains an invariant submanifold defined by $\mathbf{p} = 0$ on which the system follows the deterministic dynamics $\dot{\Psi} = F(\Psi)$.
- 2. The fixed points of Eq. (40) retains the deterministic fixed points with zero conjugate momentum: $(\Psi, \mathbf{p}) = (\mathcal{O}, 0), (\mathcal{U}, 0), (\mathcal{S}, 0).$
- 3. The Jacobian of Eq. (40) at the above fixed points is of the form

$$J(\cdot,0) = \begin{bmatrix} \nabla F(\cdot) & \Sigma^{-1} \\ 0 & -\nabla F^{T}(\cdot) \end{bmatrix}. \tag{43}$$

It follows from these properties that if we let λ_1, λ_2 denote the eigenvalues of $\nabla F(\cdot)$ then $\pm \lambda_1, \pm \lambda_2$ are eigenvalues of $J(\cdot, 0)$. Thus, for every stable (unstable) manifold at $\mathcal O$ of the deterministic dynamics there is a corresponding unstable (stable) manifold.

Finally, we conclude this brief overview of the Freidlin-Wentzell theory with a discussion of the numerical technique we use to compute most probable transition paths. Since Eq. (27) is a low dimensional system with a simple set of fixed points, we will numerically solve

the boundary value problem given by Eq. (39) with the boundary conditions $\Psi(\tau_0)=\mathcal{O}$ and $\Psi(\tau_f)=\mathcal{U}$ by computing steady states of the corresponding gradient flow. Specifically, we introduce an artificial time s and consider the evolution equation $\partial_s\Psi=-\frac{\delta I}{\delta\Psi}$ with Dirichlet boundary conditions:

$$\frac{\partial \Psi}{\partial s} = \frac{\partial^{2} \Psi}{\partial \tau^{2}} - \nabla F(\Psi) \frac{\partial \Psi}{\partial \tau} + \Sigma^{-1} \nabla F^{T}(\Psi) \Sigma \left(\frac{\partial \Psi}{\partial \tau} - F(\Psi) \right),$$

$$\Psi(s, \tau_{0}) = \mathcal{O} \text{ and } \Psi(s, \tau_{0}) = S.$$
(44)

The rate functional I acts as a Lyapunov functional in the sense that solutions of Eq. (44) satisfy $\frac{d}{ds}I[\Psi(s,\tau)] \leq 0$ and $\frac{d}{ds}I[\Psi(s,\tau)] = 0$ if and only if $\Psi(s,\tau)$ solves the Euler–Lagrange equations given in Eq. (39). Consequently, most probable transition paths $\Psi^*(\tau)$ can be computed as the stationary solutions of Eq. (44), i.e., $\lim_{s\to\infty} \Psi(s,\tau) = \Psi^*(\tau)$.

4.2. Most probable transition paths for the tropical cyclone model

We now apply the above framework to quantify the susceptibility of $\mathcal O$ to noise-induced tipping. In Fig. 6 we plot numerical approximations of the most probable transition paths computed as the stationary states of Eq. (44). From this figure we do indeed see that the most probable transition path from $\mathcal O$ to $\mathcal S$ remains close to the center manifold near $\mathcal O$. In this subsection we will validate this claim by finding an explicit formula for an approximation of the most probable path near the origin and use Eq. (35) to compute a scaling law for the expected tipping time. Specifically, we will use the Hamiltonian formulation to approximate candidates for the heteroclinic orbit that exits $\mathcal O$ and terminates at $\mathcal S$.

First, we note that the Jacobian of Eq. (40) at \mathcal{O} is given by

$$\nabla F(\mathcal{O}) = \begin{bmatrix} 0 & 0 \\ 1 & -c \end{bmatrix} \tag{45}$$

and therefore the eigenvalues of $J(\mathcal{O},0)$ are $\pm c$ and 0 with 0 having algebraic multiplicity two and geometric multiplicity one. Consequently, at $(\mathcal{O},0)$ there is a one-dimensional unstable manifold \mathcal{W}^U , a one-dimensional stable manifold \mathcal{W}^S which overlaps with the stable manifold for the deterministic dynamics, and a two-dimensional center manifold \mathcal{W}^C . Consequently, natural candidates for a heteroclinic orbit lie in \mathcal{W}^U or \mathcal{W}^C . However, we numerically found that \mathcal{W}^U does not intersect the stable manifold of \mathcal{U} and thus we focus on trajectories in \mathcal{W}^C .

To begin computing the dynamics on \mathcal{W}^C we perform a standard center manifold reduction. That is, we assume that $(\mathcal{O},0)$ can be locally parameterized as the graph of (ψ_1,p_1) , i.e., $\mathcal{W}^C=(\psi_1,\psi_2(\psi_1,p_1),p_1,p_2(\psi_1,p_1))$ where $\psi_2(\psi_1,p_1)$, $p_2(\psi_1,p_1)$ are analytic functions with power series of the form

$$\psi_{2}(\psi_{1}, p_{1}) = \sum_{i=1}^{\infty} \sum_{j=0}^{i} a_{i,j} \psi_{1}^{i-j} p_{1}^{j},
p_{2}(\psi_{1}, p_{1}) = \sum_{i=1}^{\infty} \sum_{j=0}^{i} b_{i,j} \psi_{1}^{i-j} p_{1}^{j}.$$
(46)

To determine the coefficients of the linear terms, note that W^C is tangent to the plane $E_C = \operatorname{span}\{\mathbf{v}_1, \mathbf{v}_2\}$ where

$$\mathbf{v}_{1} = \begin{bmatrix} c \\ 1 \\ 0 \\ 0 \end{bmatrix} \text{ and } \mathbf{v}_{2} = \begin{bmatrix} \sigma_{1}^{2}/c \\ 0 \\ 1 \\ 0 \end{bmatrix}$$
 (47)

are, respectively, the eigenvector and generalized eigenvector of the 0 eigenvalue of $J(\mathcal{O},0)$. Computing the tangent vectors of \mathcal{W}^C in the coordinate directions, we have that

$$\begin{bmatrix} 1 \\ a_{1,0} \\ 0 \\ b_{1,0} \end{bmatrix}, \begin{bmatrix} 0 \\ a_{1,1} \\ 1 \\ b_{1,1} \end{bmatrix} \in \operatorname{span} \left\{ \begin{bmatrix} c \\ 1 \\ 0 \\ 0 \end{bmatrix}, \begin{bmatrix} \sigma_1^2/c \\ 0 \\ 1 \\ 0 \end{bmatrix} \right\}$$

$$(48)$$

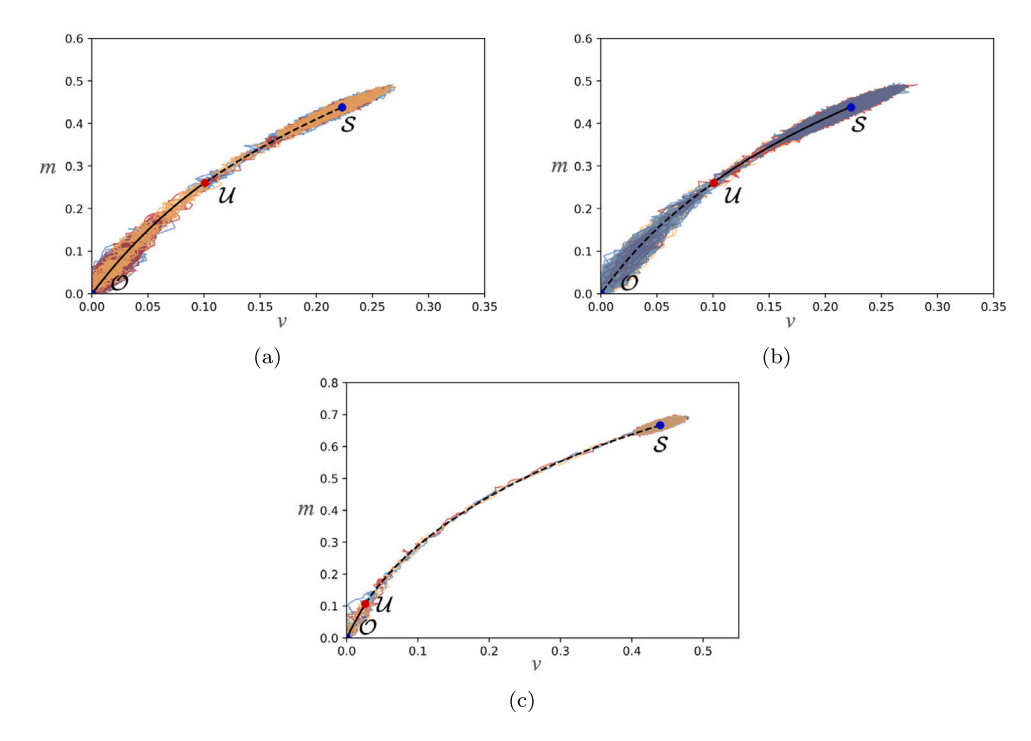


Fig. 6. Plots of the most probable path using a combination of the gradient flow and the deterministic dynamics, overlaid on realizations of Eq. (27) generated with the Euler–Maruyama method with $\tau_f = 10^6$ and $d\tau = 0.1$. The blue circles correspond to the stable fixed points, \mathcal{O}, S and the red circle corresponds to the saddle, \mathcal{V} . The solid black curve represents the piece of the most probable path from the gradient flow and the dashed black curve represents the piece of the most probable path coming from the deterministic dynamics. Parameter values are set as $\sigma_1 = \sigma_2 = .005, \gamma = 0.43, V_\rho = 10$, and c varies per plot. (a) c = 0.286. The most probable path from the non-storm state, \mathcal{O} , to the stable storm state, S, overlaid on the tipped realizations. (b) c = 0.286. The most probable path from the non-storm state, \mathcal{O} , to the stable storm state, S, overlaid on the tipped realizations.

and thus $a_{1.0} = 1/c$, $a_{1.1} = -\sigma_1^2/c^2$, $b_{1.0} = 0$, and $b_{1.1} = 0$.

Since the linear terms in the expansion of p_2 were 0, we need to compute higher order terms to obtain a non-trivial expansion. By the chain rule we have that

$$\frac{d}{d\tau}\psi_2 = \frac{\partial\psi_2}{\partial\psi_1}\frac{d\psi_1}{d\tau} + \frac{\partial\psi_2}{\partial p_1}\frac{dp_1}{d\tau},$$

$$\frac{d}{d\tau}p_2 = \frac{\partial p_2}{\partial\psi_1}\frac{d\psi_1}{d\tau} + \frac{\partial p_2}{\partial p_1}\frac{dp_1}{d\tau},$$
(49)

and thus by Eq. (40) we obtain the following system of equations

$$g + \sigma_2^2 p_2 = \frac{\partial \psi_2}{\partial \psi_1} (f + \sigma_1^2 p_1) - \frac{\partial \psi_2}{\partial p_1} \left(\frac{\partial f}{\partial \psi_1} p_1 + \frac{\partial g}{\partial \psi_1} p_2 \right),$$

$$- \frac{\partial f}{\partial \psi_2} p_1 - \frac{\partial g}{\partial \psi_2} p_2 = \frac{\partial p_2}{\partial \psi_1} (f + \sigma_1^2 p_1) - \frac{\partial p_2}{\partial p_1} \left(\frac{\partial f}{\partial \psi_1} p_1 + \frac{\partial g}{\partial \psi_1} p_2 \right),$$
(50)

where we have suppressed the independent variables to reduce the complexity of the expressions. Therefore, substituting Eq. (46) into Eq. (50) and equating powers, we can obtain linear equations for the undetermined coefficients. Following this procedure, we obtain to cubic order the following approximations

$$\psi_{2}(\psi_{1}, p_{1}) \approx \frac{1}{c}\psi_{1} - \frac{(1-\gamma)}{c^{5}}\psi_{1}^{3} - \frac{\sigma_{1}^{2}}{c^{2}}p_{1} - \frac{3\sigma_{1}^{4}}{c^{4}}p_{1}^{2} + \frac{3\sigma_{1}^{2}}{c^{3}}p_{1}\psi_{1},
p_{2}(\psi_{1}, p_{1}) \approx \frac{3(1-\gamma)\sigma_{1}^{4}}{c^{5}}p_{1}^{3} + \frac{3(1-\gamma)}{c^{3}}p_{1}\psi_{1}^{2}.$$
(51)

Note, as expected, on the sub-manifold $\mathbf{p}=0$ we recover the approximation to the center manifold for the deterministic dynamics presented in Section 2.

To compute a local approximation of the most probable transition path, we now calculate the intersection of the manifold defined by H=0 with \mathcal{W}^C . To do so, we substitute Eq. (51) into Eq. (41) and

expand

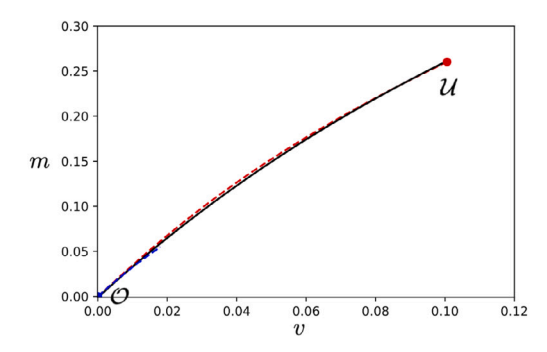
$$H(\psi_{1}, \psi_{2}(\psi_{1}, p_{1}), p_{1}, p_{2}(\psi_{1}, p_{1})) = \frac{\sigma_{1}^{2}}{2} p_{1}^{2} + \frac{\sigma_{2}^{2}}{2} p_{2}^{2}(\psi_{1}, p_{1}) + \langle F(\psi_{1}, \psi_{2}(\psi_{1}, p_{1})), (p_{1}, p_{2}(\psi_{1}, p_{2})) \rangle$$
(52)
$$\approx \frac{\sigma_{1}^{2}}{2} p_{1}^{2} - \psi_{1}^{2} p_{1}.$$

Consequently, to lowest order, the intersection of the manifold H=0 with \mathcal{W}^C corresponds to when $p_1=0$ or $p_1=2\sigma_1^{-2}\psi_1^2$. Therefore, the intersection forms two curves given (locally) by the following parameterizations:

$$(\Psi_1^*(s), \mathbf{p}_1^*(s)) = \left(s, \frac{1}{c}s - \frac{(1-\gamma)}{c^5}s^3, 0, 0\right),$$

$$(\Psi_2^*(s), \mathbf{p}_2^*(s)) = \left(s, \frac{1}{c}s - \frac{2}{c^2}s^2 - \frac{(1-\gamma)}{c^5}s^3 + \frac{6}{c^3}s^3, \frac{2}{c}s^2, \frac{6(1-\gamma)}{c^3\sigma_1^2}s^4\right).$$
(53)

The curve $(\Psi_1^*(s), \mathbf{p}_1^*(s))$ is simply the local approximation of the center manifold for the deterministic dynamics we found in Section 2. The second curve $(\Psi_2^*(s), \mathbf{p}_2^*(s))$ is the trajectory exiting $(\mathcal{O}, 0)$ that we are looking for as it is a local approximation of the heteroclinic orbit. Note, in the first two components (Ψ_1^*, p_1^*) and (Ψ_2^*, p_2^*) agree at the linear order and thus, as we suspected, the most probable transition path locally agrees with the center manifold of the deterministic dynamics near the origin. Indeed, in Fig. 7 we see that the numerical approximation generated by the gradient flow and $(\Psi_2^*(s), 0)$, the projection of the most probable path onto the $\mathbf{p}=0$ plane, are in excellent agreement near \mathcal{O} . Furthermore, if we identify the projection $(\Psi_2^*(s), 0)$ with its physical coordinates, we obtain the following local approximation to the most



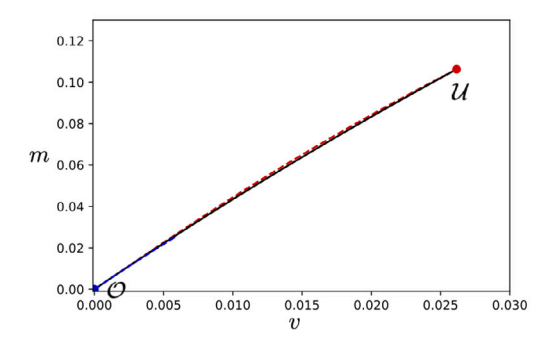


Fig. 7. Plots of the most probable path generated from the gradient flow (solid black) overlaid with the unstable manifold of \mathcal{U} (dashed red) and the approximation for the most probable path near \mathcal{O} (dashed blue), for two values of c. (a) c=0.286. (b) c=0.22.

probable path

$$m(v) = \frac{1}{c}v - \frac{2}{c^2}v^2 - \frac{(1-\gamma)}{c^5}v^3 + \frac{6}{c^3}v^3,$$
 (54)

which, at this order, does not depend on the noise components σ_1,σ_2 . Finally, to obtain an estimate for the expected tipping time we will use the above local approximation to $(\Psi_2^*(s),\mathbf{p}_2^*(s))$, given in physical coordinates by Eq. (54), and Eq. (35) to estimate the expected time of leaving a neighborhood near the origin. Specifically, it follows from the asymptotic estimate given by Eq. (9), that the v-coordinate of $\mathcal V$ scales like c^3 and thus for 0 < r < 1 we let $d = rc^3$ serve as a proxy for a typical neighborhood length scale when considering the validity of the approximation given in Eq. (54). If we let $(\Psi^*(s),\mathbf{p}^*(s))$ denote the most probable path satisfying Eq. (40), $\lim_{s\to -\infty}(\Psi^*(s),\mathbf{p}^*(s)) = (\mathcal O,0)$, and its first component ψ_1^* satisfies $\psi_1^*(0) = d$, then it follows from Eq. (42) that

$$I[\Psi^*, \mathbf{p}^*] = \int_{-\infty}^{0} \left(\left(\frac{p_1^*(s)}{\sigma_1} \right)^2 + \left(\frac{p_2^*(s)}{\sigma_2} \right)^2 \right) ds.$$
 (55)

Since we are assuming that $(\Psi^*(s), \mathbf{p}^*(s))$ is a global minimizer of the rate functional, we can use $(\Psi_2^*(s), \mathbf{p}_2^*(s))$ to obtain an upper bound on the value of $I[\Psi^*, p^*]$. Specifically, it follows from Eq. (53) that upon changing variables we have that

$$I[\Psi^*, \mathbf{p}^*] \le I[\Psi_2^*, \mathbf{p}_2^*] = \int_0^{rc^3} \left(\frac{4}{c^2 \sigma_1^2} v^4 + \frac{36(1-\gamma)^2}{c^6 \sigma_1^4 \sigma_2^2} v^8 \right) \left| \frac{ds}{dv} \right| dv,$$
 (56)

where by Eq. (40) we have that

$$\frac{ds}{dv} = \frac{1}{f(v, m(v)) + \frac{2\sigma_1^2}{c}v^2}$$
 (57)

with m(v) given by Eq. (54).

To obtain a scaling law for the right hand side of Eq. (56) we can expand in v and then integrate. Expanding in v we have that

$$\begin{split} \int_0^{rc^3} \frac{4}{c^2 \sigma_1^2} v^4 \left| \frac{ds}{dv} \right| dv &= \int_0^{rc^3} \frac{4v^2}{c \sigma_1^2 (c - 2\sigma_1^2)} \left(1 + (1 - \gamma) \frac{v}{(c - 2\sigma_1^2)c^2} \right. \\ &\quad + (1 - \gamma) \left(1 - \gamma \right. \\ &\quad - 6c(c - 2\sigma_1^2) \right) \left(\frac{v}{(c - 2\sigma_1^2)c^2} \right)^2 + \cdots \right) dv \\ &\quad = \frac{4r^3 c^8}{3\sigma_1^2 (c - 2\sigma_1^2)} + O(r^4) \end{split}$$

and

$$\begin{split} \int_0^{rc^3} \frac{36(1-\gamma)^2}{c^6\sigma_1^4\sigma_2^2} v^8 \left| \frac{ds}{dv} \right| dv &= \int_0^{rc^3} \frac{36(1-\gamma)^2 v^6}{c^5\sigma_1^4\sigma_2^2(c-2\sigma_1^2)} \left(1 + (1-\gamma) \frac{v}{(c-2\sigma_1^2)c^2} \right. \\ & + (1-\gamma) \left(1 - \gamma - 6c(c-2\sigma_1^2) \right) \left(\frac{v}{(c-2\sigma_1^2)c^2} \right)^2 + \cdots \right) dv \\ &= \frac{36r^7 c^{15}}{7\sigma_1^4\sigma_2^2(c-2\sigma_1^2)} + O(r^8). \end{split}$$

Since we are assuming $\sigma_1, \sigma_2 \ll 1$ we have that

$$I[\Psi_2^*, \mathbf{p}_2^*] \sim \frac{4}{3} \frac{r^3 c^7}{\sigma_1^2} + \frac{36}{7} \left(\frac{r^3 c^7}{\sigma_1^2}\right)^2 \frac{c}{\sigma_2^2}.$$

Therefore, we obtain the following scaling law (up to logarithmic equivalence) for the expected tipping time from this neighborhood

$$\mathbb{E}[\tau_r^*] \approx \exp(I[\boldsymbol{\varPsi}^*, \mathbf{p}^*]) \lesssim \exp\left(\frac{4}{3} \frac{r^3 c^7}{\sigma_1^2} + \frac{36}{7} \frac{c}{\sigma_2^2} \left(\frac{r^3 c^7}{\sigma_1^2}\right)^2\right),\tag{58}$$

where τ_r^* is the stopping time to leave this neighborhood.

The scaling law given in Eq. (58) is interesting in that it illustrates the interplay between the dimensionless sheer c and σ_1,σ_2 . Namely, it identifies the two dimensionless measures of noise strength $\tilde{\sigma}_1^2 = \sigma_1^2/c^7$ and $\tilde{\sigma}_2^2 = \sigma_2^2/c$ which control the tipping time. In particular, it provides further evidence for why tipping near the origin is far more common than tipping away from the stable storm state S. Indeed, for the numerical experiments presented in Fig. 5, the ratio c^7/σ_1^2 ranges from (approximately) 1 to 6, i.e., is $\mathcal{O}(1)$ despite $\sigma_1 = \sigma_2 \sim 10^{-3}$.

5. Discussion

An analysis of the various tipping mechanisms for a low-dimensional model of a tropical cyclone show a range of different possibilities for both the formation and destruction of a hurricane. The key results are the following:

- The non-storm state O is a base state that is asymptotically stable
 for all parameter values. Consequently, there is no possibility of
 bifurcation-induced tipping away from it to an activated storm
 state. Furthermore, it does not move in phase space and thus
 there is no rate-induced tipping that would form a stable storm
 state from a non-storm state.
- 2. The dimensionless wind shear acts as a natural bifurcation parameter: with increasing values of *c* there is a saddle–node bifurcation in which the stable storm state is eliminated. That is to say that excessive wind shear kills a storm in the sense that it will no longer be able to maintain itself for a prolonged period of time. Thus, in order for the formation of a tropical cyclone to occur, we need sufficiently low wind shear, corroborating physical observations [46].
- 3. A necessary condition for the destabilization of the stable storm state, through rate-induced tipping, is that both the potential velocity V_p and dimensionless wind shear c need to be increasing in time. This is counter-intuitive as the energy source is encoded in the maximum potential velocity in this model and thus it would be expected that increasing this quantity might strengthen the cyclone. But we show that, as long as it is accompanied by a sufficient wind shear, it serves to kill the hurricane, and the increase of wind shear cannot achieve that alone.

- 4. We showed that the non-storm is state is highly susceptible to noise-induced tipping while the stable storm state is robust to random fluctuations. This susceptibility was quantified by the ratio c^7/σ_1^2 which is a dimensionless measure of the interplay between wind shear and noise. Note, this result was dependent on the assumption of additive noise, the use of reflecting boundary conditions, and the specific nonlinearities in Eq. (2). We were primarily interested in studying this problem from a mathematical viewpoint and thus introduced additive noise as a simplifying assumption. For a specific application, a more careful introduction of noise would require one to revisit the derivation presented in [39,40] and determine how uncertainty could be more realistically introduced into the model. It is an interesting question as to how the resulting form of the noise would modify the expected tipping time and in particular the susceptibility of the non-storm state to noise induced tipping. The particular polynomial form of the nonlinearities also plays a key role in this scaling law. It would be an interesting mathematical question to consider more generic systems with a non-trivial center manifold in order to provide more intuition for the mechanisms that dictate the algebraic structure of the scaling law. Indeed, providing some intuition for why we obtain such a large power in c would be useful in broader contexts.
- 5. We identified that the most probable transition path for noiseinduced tipping from \mathcal{O} closely tracks the center manifold for the deterministic dynamics. That is, the center manifold is a region in phase space that is most vulnerable to random fluctuations. Note, this result and the definition of most probable transition path we have employed relied on the assumption that σ is asymptotically small. However, for nonzero noise the local maximum of the stationary distribution for the system may be shifted away from the equilibrium, thus influencing the most probable transition paths and the expected tipping time. For example, when converting the system $dx = -xdt + \sigma dW$, dy = $-ydt + \sigma dW$ to polar coordinates $r^2 = x^2 + y^2$, $\tan(\theta) = y/x$, one obtains $dr = (-r + \sigma^2/(2r))dt + \sigma dW$ and thus the stationary density will be concentrated around a circle of radius $r = \sigma/\sqrt{2}$; see Example 4.5.5 in [47]. Given that \mathcal{O} is highly susceptible to noise induced tipping, perhaps more sophisticated analysis needs to be done in order to determine more precise scaling laws for the expected tipping time. Indeed, transition path theory allows for the computation of reaction rates (inverse of expected tipping times) [48,49]. Additionally, more refined asymptotic estimates of the expected tipping time can be computed through more careful analysis of the prefactor that is lost in the statement of logarithmic equivalence in Eq. (35) [50].

As is standard in this type of analysis, we considered these various tipping mechanisms independent of one another. A natural question is how do these various mechanisms couple to induce a storm-state or destabilize a storm. A natural extension of the analysis presented in this paper is to ask how the interplay of a parameter shift and additive noise will affect tipping within the system. Based on the work and analysis in [26,51], we expect that in tipping away from the stable storm state, there will be an interplay between the rate and noise-induced tipping mechanisms, and the additive noise will lower the critical rate needed for tipping. Additionally, tipping should occur away from the non-storm state, but as there was no rate-induced tipping with this initialization, we must explore if there is an interplay of the tipping mechanisms.

Using the same additive noise and ramp parameter as in prior sections, the natural system to study this interaction is given by

$$\begin{split} dv &= \left(\frac{(1-\gamma)V_p(A(s))^2}{V_p^{-2}}m^3 - (1-\gamma m^3)v^2\right)d\tau + \sigma_1 dW_1,\\ dm &= \left((1-m)v - c(A(s))\right)d\tau + \sigma_2 dW_2,\\ ds &= d\tau. \end{split} \tag{59}$$

While we would like to use the methods employed in [51] and [52]. the center manifold of the non-storm state, as described in Section 2, demands a more careful approach, and is beyond the scope of the current study. Nevertheless, when conducting Monte-Carlo simulations of Eq. (59) we noticed some interesting phenomena that have led to further conjectures. First, initializing at the stable storm state corresponding to the start of the ramp function, we see in Fig. 8(a) that for $r < r_c$, with the addition of noise, there is tipping to the nonstorm state. Notice there is an interplay between these two mechanisms. Initializing at the non-storm state corresponding to the start of the ramp, we see in Fig. 8(b) that there is tipping to the stable storm state. Note, in Fig. 8(b), realizations that tip actually begin by tipping to the stable storm state corresponding to the start of the ramp function, and then end-point track to the stable storm state corresponding to the end of the ramp function. This implies the two tipping mechanisms are not interacting to induce tipping: noise-induced tipping occurs first, followed by tracking of the stable storm state from the parameter shift. While we illustrate this phenomenon for one set of noise strengths and a rate parameter, this behavior held true for multiple sets of parameter values.

To validate the above conjectures requires an adaptation of the standard Freidlin–Wentzell theory of large deviations to non-autonomous systems. One approach is to first follow the procedure in [42] and "compactify" the system in such a way that compact invariant sets such as equilibria now describe the long time behavior of the system. Noise-induced tipping can now be studied on the compactified system using the standard Freidlin–Wentzell theory of large deviations. When considering the various tipping phenomenon, this system will now contain multiple scales, e.g. r, c^7/σ_1^2 , and c/c_2^2 , and it would be interesting to understand how these various parameters influence tipping phenomenon. From a variational perspective, Γ -convergence provides a natural tool for studying the minimizers of the Freidlin–Wentzell functional in various asymptotic limits.

Declaration of competing interest

The authors declare that they have no known competing financial interests or personal relationships that could have appeared to influence the work reported in this paper.

Data availability

No data was used for the research described in the article.

Acknowledgments

The authors sincerely thank the anonymous referees for taking the time to carefully read this manuscript. We believe their comments and suggestions greatly improved the quality of this work. The authors would also like to thank Anthony Roberts for his informal comments which helped clarify our understanding of center manifolds. Finally, the authors would like to acknowledge support of the Mathematics and Climate Research Network (MCRN) under NSF grant DMS-1722578. Katherine Slyman and Christopher Jones were additionally supported by Office of Naval Research grant N000141812204.

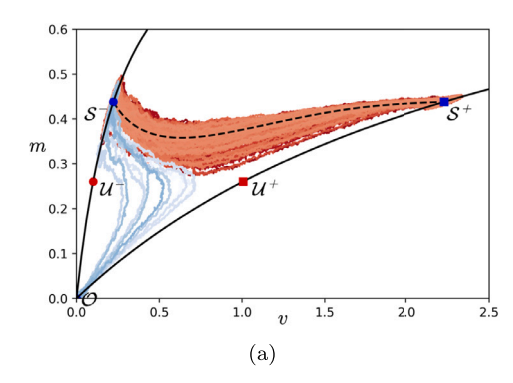
Appendix A. Center manifold approximation of the origin

To determine an approximation of the center manifold at $\mathcal O$ for Eq. (3) we follow [53] and consider a solution of the form

$$m = h(v) = \sum_{k=1}^{n} a_k v^k. \tag{A.1}$$

Differentiating Eq. (A.1) with respect to v, it follows from Eq. (3) that

$$g(v, h(v)) = \frac{dm}{d\tau} = h_v(v)\frac{dv}{d\tau} = h_v(v)f(v, h(v)). \tag{A.2}$$



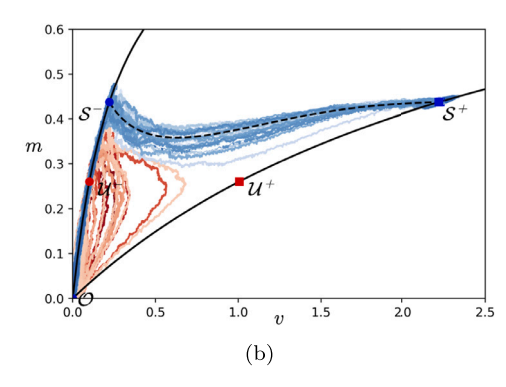


Fig. 8. Realizations of the system given in Eq. (59), solved with the Euler–Maruyama method with $\tau_f = 2500, d\tau = 0.1$. Parameter values are set as $\sigma_1 = \sigma_2 = 0.005, r = .03, \gamma = 0.43$, and V_p, c are time-dependent and defined as in Eqs. (23), (24), and (25). The three fixed points at the start of the ramp, \mathcal{O}, U^-, S^- , correspond to the non-storm state, the unstable storm state, and the stable storm state. These stable fixed points are denoted by blue circles and the saddle node is denoted by a red circle. The three fixed points at the end of the ramp, \mathcal{O}, U^+, S^+ , correspond to the non-storm state, the unstable storm state, and the stable storm state. These stable fixed points are denoted by blue squares and the saddle node is denoted by a red square. The solid black curves correspond to the m nullcline at the start and the end of the ramp function. The dashed black curves correspond to the solution in the deterministic system ($\sigma_1 = \sigma_2 = 0$). (a) 1000 realizations initialized at the stable storm state, S^- . The blue realizations tip from S^- to S^+ , and do not tip. (b) 1000 realizations initialized at the non-storm state, S^- . The blue realizations tip from S^- to S^+ . The red realizations do not tip.

However from Eq. (3) we also know that $\dot{m} = g(v, h(v))$. Therefore, assuming n = 5 and equating powers of v in the equation $h_v(v)f(v, h(v)) = g(v, h(v))$ we arrive at

$$a_{1} = \frac{1}{c},$$

$$a_{2} = 0,$$

$$a_{3} = \frac{\gamma - 1}{c^{5}},$$

$$a_{4} = \frac{2(\gamma - 1)}{c^{6}},$$

$$a_{5} = \frac{6 - 6c^{2} - 12\gamma + 6c^{2}\gamma - c^{4}\gamma + 6\gamma^{2}}{c^{9}}$$
(A.3)

and thus $m(v) = a_1v + a_2v^2 + a_3v^3 + a_4v^4 + a_5v^5$ is the desired approximation of the center manifold for Eq. (3) near \mathcal{O} .

Appendix B. Stability of the origin

From Appendix A, we found a center manifold approximation near \mathcal{O} given by

$$m(v) = \frac{1}{c}v + \frac{\gamma - 1}{c^5}v^3 + \frac{2(\gamma - 1)}{c^6}v^4 + O(v^5).$$
(B.1)

If we consider Eq. (3), we can use $\frac{dv}{d\tau}$ as a differential equation for the dynamics of the center manifold by replacing m with m(v), resulting in

$$\frac{dv}{d\tau} = (1 - \gamma)(m(v))^3 - (1 - \gamma(m(v))^3)v^2
= -v^2 + O(v^3).$$
(B.2)

Since the coefficient of v^2 is negative, it follows that the origin is an asymptotically stable fixed point for the center manifold and hence for the original system in Eq. (3).

Appendix C. Proof of Proposition 3.8

Proof. We want to show that the box $K_{a,b} = [a_1, b_1] \times [a_2, b_2]$ is forward invariant with respect to the flow, and therefore we need to find the direction of the flow on the four sides of the box.

• Side 1 $(v = a_1, m \in [a_2, b_2])$:

$$\dot{v} = (1 - \gamma) \left(\frac{V_p}{V_p^-}\right)^2 m^3 - (1 - \gamma m^3) a_1^2$$

$$= m^3 \left((1 - \gamma) \left(\frac{V_p}{V_p^-}\right)^2 + \gamma a_1^2\right) - a_1^2$$

$$\geq a_2^3 \left((1 - \gamma) \left(\frac{V_p}{V_p^-}\right)^2 + \gamma a_1^2\right) - a_1^2$$

$$> 0.$$
(C.1)

since
$$\sqrt[3]{\frac{a_1^2}{(1-\gamma)\left(\frac{V_p}{V_-}\right)^2 + \gamma a_1^2}} < a_2$$
.

• Side 2 ($v \in [a_1, b_1], m = a_2$):

$$\dot{m} = (1 - a_2)v - ca_2
\ge (1 - a_2)a_1 - ca_2
= a_1 - (a_1 + c)a_2$$
(C.2)

since $a_2 < \frac{a_1}{a_1+c}$.

• Side 3 ($v = b_1, m \in [a_2, b_2]$):

$$\dot{v} = (1 - \gamma) \left(\frac{V_p}{V_p^-}\right)^2 m^3 - (1 - \gamma m^3) b_1^2$$

$$= m^3 \left((1 - \gamma) \left(\frac{V_p}{V_p^-}\right)^2 + \gamma b_1^2\right) - b_1^2$$

$$\leq b_2^3 \left((1 - \gamma) \left(\frac{V_p}{V_p^-}\right)^2 + \gamma b_1^2\right) - b_1^2$$

$$\leq 0$$
(C.3)

since
$$b_2 < \sqrt[3]{\frac{b_1^2}{(1-\gamma)\left(\frac{V_p}{V_2}\right)^2 + \gamma b_1^2}}$$
.

• Side 4
$$(v \in [a_1, b_1], m = b_2)$$
:

$$\dot{m} = (1 - b_2)v - cb_2$$

$$\leq (1 - b_2)b_1 - cb_2$$

$$= b_1 - (b_1 + c)b_2$$

$$< 0,$$
since $\frac{b_1}{b_1 + c} < b_2$. \square

References

- [1] P. Ashwin, C. Perryman, S. Wieczorek, Parameter shifts for nonautonomous systems in low dimension: Bifurcation-and rate-induced tipping, Nonlinearity 30 (6) (2017) 2185.
- [2] T. Lenton, H. Held, E. Kriegler, J. Hall, W. Lucht, S. Rahmstorf, H. Schellnhuber, Tipping elements in the Earth's climate system, Proc. Natl. Acad. Sci. 105 (6) (2008) 1786–1793.
- [3] T.M. Lenton, J. Rockström, O. Gaffney, S. Rahmstorf, K. Richardson, W. Steffen, H.J. Schellnhuber, Climate tipping points—too risky to bet against, Nature 575 (7784) (2019) 592–595.
- [4] L. Kemp, C. Xu, J. Depledge, K. Ebi, G. Gibbins, T. Kohler, J. Rockstrom, M. Scheffer, H. Schellnhuber, W. Steffen, T. Lenton, Climate endgame: Exploring catastrophic climate change scenarios, Proc. Natl. Acad. Sci. 119 (34) (2022) e2108146119.
- [5] N. Berglund, B. Gentz, Metastability in simple climate models: Pathwise analysis of slowly driven Langevin equations, Stoch. Dyn. 2 (03) (2002) 327–356.
- [6] I. Eisenman, J. Wettlaufer, Nonlinear threshold behavior during the loss of Arctic sea ice, Proc. Natl. Acad. Sci. 106 (1) (2009) 28–32.
- [7] S. Wieczorek, P. Ashwin, C. Luke, P. Cox, Excitability in ramped systems: the compost-bomb instability, Proc. R. Soc. A Math. Phys. Eng. Sci. 467 (2129) (2010) 1243–1269.
- [8] I. Eisenman, Factors controlling the bifurcation structure of sea ice retreat, J. Geophys. Res.: Atmos. 117 (D1) (2012).
- [9] D. Rothman, Characteristic disruptions of an excitable carbon cycle, Proc. Natl. Acad. Sci. 116 (30) (2019) 14813–14822.
- [10] C. Arnscheidt, D. Rothman, Routes to global glaciation, Proc. R. Soc. Lond. Ser. A Math. Phys. Eng. Sci. 476 (2239) (2020).
- [11] J. Lohmann, P. Ditlevsen, Risk of tipping the overturning circulation due to increasing rates of ice melt, Proc. Natl. Acad. Sci. 118 (9) (2021) e2017989118.
- [12] A. Vanselow, S. Wieczorek, U. Feudel, When very slow is too fast-collapse of a Predator-Prey system, J. Theoret. Biol. 479 (2019) 64–72.
- [13] P. O'Keeffe, S. Wieczorek, Tipping phenomena and points of no return in ecosystems: Beyond classical bifurcations, SIAM J. Appl. Dyn. Syst. 19 (4) (2020) 2371–2402.
- [14] J. Drake, B. Griffen, Early warning signals of extinction in deteriorating environments, Nature 467 (7314) (2010) 456–459.
- [15] M. Scheffer, E. Van Nes, M. Holmgren, T. Hughes, Pulse-driven loss of top-down control: the critical-rate hypothesis, Ecosystems 11 (2) (2008) 226–237.
- [16] E. Forgoston, S. Bianco, L. Shaw, I. Schwartz, Maximal sensitive dependence and the optimal path to epidemic extinction, Bull. Math. Biol. 73 (3) (2011) 495–514.
- [17] I. Schwartz, E. Forgoston, S. Bianco, L. Shaw, Converging towards the optimal path to extinction, J. R. Soc. Interface 8 (65) (2011) 1699–1707.
- [18] L. Billings, E. Forgoston, Seasonal forcing in stochastic epidemiology models, Ricerche di Matematica 67 (1) (2018) 27–47.
- [19] J. Hindes, I. Schwartz, Rare events in networks with internal and external noise, Europhys. Lett. 120 (5) (2018) 56004.
- [20] J. Andreoni, N. Nikiforakis, S. Siegenthaler, Predicting social tipping and norm change in controlled experiments, Proc. Natl. Acad. Sci. 118 (16) (2021) e2014893118.
- [21] J. Andreoni, N. Nikiforakis, S. Siegenthaler, Social tipping points and forecasting norm change, in: CEPR, 2021, [Online]).
- [22] P. Ashwin, S. Wieczorek, R. Vitolo, P. Cox, Tipping points in open systems: Bifurcation, noise-induced and rate-dependent examples in the climate system, Phil. Trans. R. Soc. A 370 (1962) (2012) 1166–1184.
- [23] J. Thompson, J. Sieber, Predicting climate tipping as a noisy bifurcation: A review, Int. J. Bifurcation Chaos 21 (02) (2011) 399–423.

- [24] T. Lenton, Early warning of climate tipping points, Nature Clim. Change 1 (4) (2011) 201.
- [25] T. Lenton, V. Livina, V. Dakos, E. Van Nes, M. Scheffer, Early warning of climate tipping points from critical slowing down: Comparing methods to improve robustness, Phil. Trans. R. Soc. A 370 (1962) (2012) 1185–1204.
- [26] P. Ritchie, J. Sieber, Early-warning indicators for rate-induced tipping, Chaos 26 (9) (2016) 093116.
- [27] S. Wieczorek, C. Xie, P. Ashwin, Rate-induced tipping: Thresholds, edge states and connecting orbits, Nonlinearity 36 (6) (2023) 3238.
- [28] E. Forgoston, R.O. Moore, A primer on noise-induced transitions in applied dynamical systems, SIAM Rev. 60 (4) (2018) 969–1009.
- [29] N. Berglund, Kramers' law: validity, derivations and generalisations, Markov Process Relat. Fields 19 (3) (2013) 459–490.
- [30] M.I. Freidlin, A.D. Wentzell, Random Perturbations of Dynamical Systems, Vol. 260, Springer Science & Business Media, 2012.
- [31] N. Mori, T. Takemi, Y. Tachikawa, H. Tatano, T. Shimura, T. Tanaka, T. Fujimi, Y. Osakada, A. Webb, E. Nakakita, Recent nationwide climate change impact assessments of natural hazards in Japan and east Asia, Weather Clim. Extrem. 32 (2021) 100309.
- [32] C. Dahlgren, K. Sherman, Preliminary Assessment of Hurricane Dorian's Impact on Coral Reefs of Abaco and Grand Bahama, Perry Institute of Marine Science Report to the Government of The Bahamas, 2020.
- [33] A. Graumann, T.G. Houston, J.H. Lawrimore, D.H. Levinson, N. Lott, S. McCown, S. Stephens, D.B. Wuertz, Hurricane Katrina: a Climatological Perspective: Preliminary Report, US Department of Commerce, National Oceanic and Atmospheric Administration, National Environmental Satellite Data and Information Service, National Climatic Data Center, 2006.
- [34] L. Bengtsson, Hurricane threats, Science 293 (5529) (2001) 440-441.
- [35] D.A. Zelinsky, Tropical cyclone report: Hurricane lorenzo, in: NOAA/NHC, 2019.
- [36] B. van der Bolt, E.H. van Nes, Understanding the critical rate of environmental change for ecosystems, cyanobacteria as an example, PLoS One 16 (6) (2021) e0253003.
- [37] K.A. Emanuel, The theory of hurricanes, Annu. Rev. Fluid Mech. 23 (1) (1991) 179–196.
- [38] K. Emanuel, Hurricanes: Tempests in a greenhouse, Phys. Today 59 (8) (2006) 74–75.
- [39] K. Emanuel, Self-stratification of tropical cyclone outflow, Part II: Implications for storm intensification, J. Atmosph. Sci. 69 (3) (2012) 988–996.
- [40] K. Emanuel, F. Zhang, The role of inner-core moisture in tropical cyclone predictability and practical forecast skill, J. Atmos. Sci. 74 (7) (2017) 2315–2324.
- [41] K. Emanuel, A fast intensity simulator for tropical cyclone risk analysis, Nat. Hazards 88 (2) (2017) 779–796.
- [42] S. Wieczorek, C. Xie, C.K. Jones, Compactification for asymptotically autonomous dynamical systems: theory, applications and invariant manifolds, Nonlinearity 34 (5) (2021) 2970.
- [43] C. Kiers, C.K. Jones, On conditions for rate-induced tipping in multi-dimensional dynamical systems, J. Dynam. Differential Equations 32 (2020) 483–503.
- [44] V.M. Gálfi, V. Lucarini, F. Ragone, J. Wouters, Applications of large deviation theory in geophysical fluid dynamics and climate science, La Rivista del Nuovo Cimento 44 (6) (2021) 291–363.
- [45] M. Heymann, E. Vanden-Eijnden, The geometric minimum action method: A least action principle on the space of curves, Commun. Pure Appl. Math.: A J. Issued by Courant Inst. Math. Sci. 61 (8) (2008) 1052–1117.
- [46] W.M. Frank, E.A. Ritchie, Effects of vertical wind shear on the intensity and structure of numerically simulated hurricanes, Mon. Weather Rev. 129 (9) (2001) 2249–2269
- [47] C. Gardiner, Stochastic Methods: A Handbook for the Natural and Social Sciences, fourth ed., Springer, New York, NY, 2009.
- [48] E. Vanden-Eijnden, et al., Towards a theory of transition paths, J. Stat. Phys. 123 (3) (2006) 503–523.
- [49] E. Vanden-Eijnden, et al., Transition-path theory and path-finding algorithms for the study of rare events, Ann. Rev. Phys. Chem. 61 (2010) 391–420.
- [50] T. Grafke, T. Schäfer, E. Vanden-Eijnden, Sharp asymptotic estimates for expectations, probabilities, and mean first passage times in stochastic systems with small noise, 2021, arXiv preprint arXiv:2103.04837.
- [51] K. Slyman, C.K. Jones, Rate and noise-induced tipping working in concert, Chaos 33 (1) (2023).
- [52] E. Fleurantin, K. Slyman, B. Barker, C.K. Jones, A dynamical systems approach for most probable escape paths over periodic boundaries, Physica D (2023) 133860.
- [53] J. Carr, Applications of Centre Manifold Theory, Vol. 35, Springer Science & Business Media, 2012.